JOURNAL OF MATERIALS SCIENCE 17 (1982) 1541–1570

Review
EXAFS studies in materials science

S. J. GURMAN
Department of Physics, University of Leicester, Leicester, UK

A review is given of the results obtained in the field of materials science using the comparatively new technique of Extended X-ray Absorption Fine Structure (EXAFS) spectroscopy. Particular emphasis is placed on the determination of the atomic distribution functions in amorphous and multi-component materials, especially metallic and oxide glasses, catalysts and alloys. The advantages and disadvantages of the technique compared to diffraction studies are discussed.

1. Introduction

The availability of intense sources of continuous radiation in the X-ray region of the electromagnetic spectrum at synchrotron laboratories around the world (principally at Daresbury, UK, Stanford, USA and Orsay, France) has stimulated the development of a technique for structure determination which is particularly well-suited to studies of the local atomic environment in complex systems. It is observed that the X-ray absorption cross-section for the photoexcitation of an electron from a deep core state exhibits oscillations as a function of photon energy. This structure is known as the Extended X-ray Absorption Fine Structure, or EXAFS. The oscillations are a final-state electron effect, arising from the interference between the outgoing photoelectron wavefunction and that small part of itself which is scattered back from neighbouring atoms. Thus, conceptually, EXAFS may be considered as a type of electron diffraction where the source of electrons lies within the atom which participates in the X-ray absorption event.

The primary objective of EXAFS studies is to determine the local atomic environment of the excited atom by analysing the measured oscillatory structure. The interference which gives rise to the EXAFS reflects directly the total phase-shift of the backscattered wave, which is largely made up of the product of the photoelectron wave-vector and the distance travelled, but which also includes contributions from the scattering process and from the passage of the photoelectron out and back through the potential of the excited atom. (The major contribution to the absorption matrix element comes from regions of space very close to the nucleus of the excited atom since the core state is strongly localized.) The amplitude of the oscillations depends on the number and electron scattering strength of the scattering atoms. Consequently, analysis of the EXAFS yields information not only on the distance but also on the number and chemical type of the near-neighbours of the emitting atom. Also, since the measurements relate to the absorption edge of one particular type of atom, we obtain *partial* distribution functions.

Since the EXAFS depends only on the local atomic environment, by reason of the fact that only elastically scattered electrons can contribute to the interference and that the elastic mean free path is short, it is particularly useful for the study of amorphous materials. The atom-specific nature of the process also makes it suitable for the study of complex systems, of for the determination of the environment of dilute species.

In this review, we shall first consider the fundamentals of the EXAFS process, the theoretical description which shows what information is contained within a spectrum and how it may be analysed. We will then survey the results which have been obtained by use of the technique in four areas of study which are of relevance to materials science: metallic glasses, oxide glasses (primarily silicate glasses), catalysts and dilute alloys. Other reviewers have given surveys of the use of EXAFS in the study of amorphous solids [1–3], catalysts [4] and biological molecules [5, 6]. Metallic glass structures investigated using EXAFS have been

0022–2461/82/061541–30$06.10/0

reviewed by Wong [7]. Good surveys of EXAFS theory, techniques and applications are available in the books edited by Teo and Joy [8] and by Joyner [9].

2. Basic principles of EXAFS

The attenuation of X-rays passing through a medium occurs via three principal processes: scattering, pair production and photoelectric absorption. In the energy range of interest for EXAFS studies (1 to 20 keV) photoelectric absorption dominates the attenuation process. In photoelectric absorption, a single X-ray photon is absorbed by an atom, giving up its energy to an electron which is then excited into a higher energy level. The energy balance is expressed by

$$E = \hbar\omega - E_b, \tag{1}$$

where $\hbar$ is Planck's constant divided by 2π, ω is the frequency of the incident X-ray photon, E_b is the binding energy of the electron in its initial state and E its kinetic energy after emission from the atom. We assume here that the final-state electron is unbound, i.e. that it has a continuous distribution of allowed energies: we do not consider Rydberg transitions to weakly bound states.

In order to understand the mechanism which gives rise to the EXAFS spectrum, let us consider the K adsorption edge, corresponding to excitation of an electron from the ls-level. In the dipole approximation the probability of X-ray absorption is given by [10]:

$$P = \frac{2\pi^2 e^2}{mc^2\omega} |M_{fs}|^2 \rho(E_f) \tag{2}$$

where $M_{fs} = \langle f|\boldsymbol{\varepsilon}\cdot\mathbf{r}|s\rangle . \boldsymbol{\varepsilon}|s\rangle$ is the initial ls-state, $|f\rangle$ the final state and $\rho(E_f)$ is the density of allowed states at the final state energy, E_f. e is the electronic charge, m is the electronic mass, c is the speed of light and $\boldsymbol{\varepsilon}$ is the electric field polarization vector. The selection rules in the dipole approximation force $|f\rangle$ to be a p-state if the initial state is s-like. For X-ray energies well above the absorption edge $\rho(E_f)$ is a smooth function and may be approximated by the density of states of a free electron of energy $E = E_0 + \hbar^2k^2/2m$. Here E_0 is the energy of a free electron with momentum $k = 0$ and is the effective mean potential experienced by an excited electron in the medium. It is usually called the threshold energy: it is not the same as the energy of the edge, which lies at the Fermi energy (or at least at the lowest unoccupied energy level). With this assumption for $\rho(E_f)$ the only remaining factor that can give rise to the EXAFS signal is the matrix element M_{fs}. Now, the initial state is fixed and does not vary with ω. The final state $|f\rangle$, however, varies with ω and it is this variation which gives rise to the fine structure.

The wavefunction $|f\rangle$ may be considered as a sum of two contributions. If the atom were isolated, the photoelectron would be in a solely outgoing state relative to the excited atom. In this case M_{fs} shows no fine structure and the X-ray absorption coefficient varies monotonically with ω. Such is the case for a monatomic gas such as argon. If now, the excited atom is surrounded by other atoms, as in a molecular gas or any condensed phase, the outgoing electron will be scattered by the surrounding atoms, giving rise to incoming waves. These incoming or backscattered waves can interfere constructively or destructively with the outgoing wave. This interference gives rise to an oscillatory variation in M_{fs} as a function of ω, since the wavelength of the photoelectron is a function of ω as a result of Equation 1. The significant region of space for this process is the region where $|s\rangle$ exists, close to the nucleus. Constructive interference there increases M_{fs}, and hence the absorption coefficient, whilst destructive interference lowers M_{fs} below the isolated atom value.

The absorption coefficient, $\mu(k)$, can therefore be written as

$$\mu(k) = \mu_0(k)\,[1 + \chi(k)], \tag{3}$$

where k, the photoelectron momentum, may be expressed in terms of the photoelectron energy by use of the free-electron expression given above. $\mu_0(k)$ is the smoothly varying background which physically corresponds to the absorption coefficient of the isolated atom. The fine-structure or EXAFS function arising as a consequence of the interference between backscattered and outgoing photoelectron waves is therefore defined by

$$\chi(k) = [\mu(k) - \mu_0(k)]/\mu_0(k). \tag{4}$$

We note here that $\mu_0(k)$ is only that part of the atomic absorption coefficient which is due to transitions from the inital state of interest, i.e. the contribution of one particular edge. The first step in data reduction is to remove the contributions of the other edges to the absorption coefficient, which may be done by fitting a smooth function, such as the Victoreen [11]

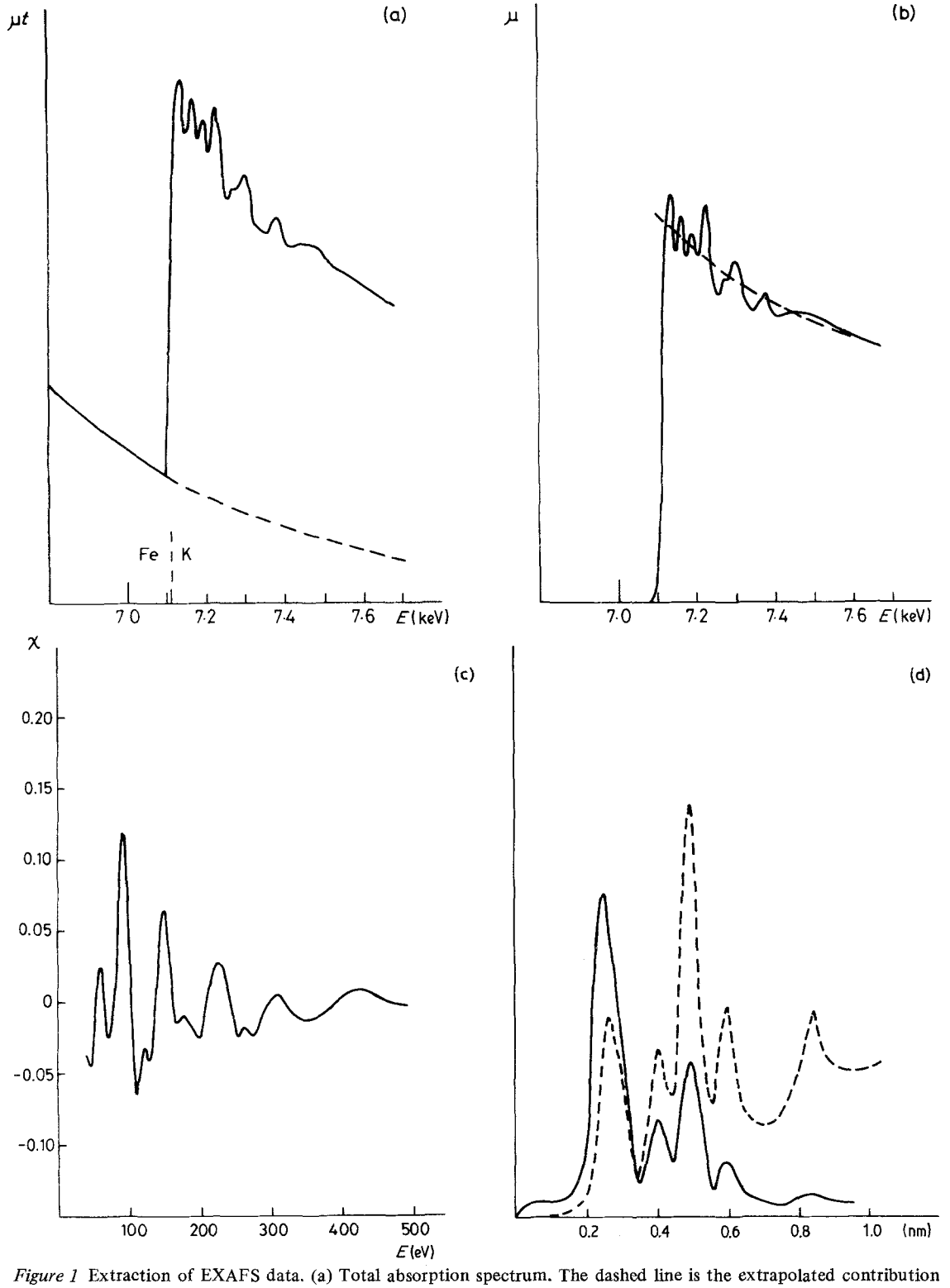

Figure 1 Extraction of EXAFS data. (a) Total absorption spectrum. The dashed line is the extrapolated contribution from lower energy edges which is subtracted from the total absorption to obtain the contribution from the edge of interest, which is shown in (b). The dashed line in (b) is the smooth atomic absorption factor μ_0: with this the EXAFS function shown in (c) may be obtained by use of Equation 3. The Fourier transform of this is shown in (d): the solid line is the F.T. of $k\chi(k)$, the dashed line R^2 times this which corresponds to the partial RDF (Equation 6) when the phase factors are taken into account.

expression, to the absorption below the edge and extrapolating to higher energies. Similarly, we obtain $\mu_0(k)$ by fitting such an expression to the edge contribution and so obtain the EXAFS function $\chi(k)$. The various stages of this process are shown in Fig. 1.

The theory of the EXAFS function itself has a long history, going back to the original work of Kronig [12–14]; indeed EXAFS is still sometimes referred to as Kronig structure. The first successful detailed theory of EXAFS, based on the physical ideas described above, was developed by Sayers, Lytle and Stern in the early 1970s [15]. This theory has subsequently been refined and generalized by several workers [16–18]. Lee and Pendry first gave a full expression for $\chi(k)$ in the case of K-shell absorption in a randomly oriented polycrystalline or amorphous sample and this takes the form

$$\chi(k) = \tfrac{2}{3}\,\mathrm{Re}\sum_m Z_{1\mathrm{m},1\mathrm{m}} \exp(2i\delta_1') \qquad (5)$$

where the elements of the matrix Z give the fraction of the wave which is backscattered. Re signifies "the real part". This theory has recently been extended to include other edges and crystal-orientation and polarization effects [18]. By approximating the photoelectron wavefront at the scattering atom by a plane wave, and repeating this process at the emitter, Z may be greatly simplified and if a further level of approximation is invoked by replacing a resultant Hankel function by its asymptotic form a much simpler expression for $\chi(k)$ results [16, 17]. Thus, except for energies close to an absorption edge, and including single scattering events only, we have:

$$\chi(k) = \sum_j \frac{N_j}{kR_j^2} |f_j(\pi)| \exp(-2\sigma_j^2 k^2) \times \exp(-2R_j/\lambda) \sin(2kR_j + 2\delta_1' + \psi_j), \qquad (6)$$

where atomic units have been used. (Atomic units are that set of units where $e = m = \hbar = 1$. Lengths are measured in Bohr radii, 1 a.u. = 0.0529 nm, and energies in Hartrees, 1 hart = 27.2 eV.) k is the momentum of the photoelectron ($k^2 = 2E$ in atomic units), N_j is the number of like atoms at a distance R_j from the emitting atom, each with a backscattering factor $f_j(\pi)$. λ is the elastic mean free path of the photoelectrons: only elastically scattered electrons can interfere. The other exponential factor is a Debye–Waller factor with σ_j^2 the mean square variation in interatomic distance between the emitting and scattering atoms. In a crystal this is due to thermal motion, but note that σ_j^2 is not equal to the sum of the mean square thermal vibration amplitudes of the two atoms because the thermal motions are to some extent correlated [19]. In an amorphous system there is an additional contribution to σ_j^2 from the static variability in the distances due to structural disorder. The Debye–Waller form is obtained under the assumption that the distribution of distances is Gaussian: this assumption is valid for thermal motion and for weak static disorder but may be poor for highly-disordered systems. This point is considered further below. δ_1' is the phase-shift produced in the passage of the photoelectron through the excited atom potential: for K-edge absorption this is the $l = 1$ phaseshift since the photoelectron must be in a p-state due to the dipole selection rules. ψ_j is the phase of the backscattering factor $f_j(\pi)$.

The great advantage EXAFS has over diffraction techniques is that we may measure the EXAFS on the absorption edges of all the different types of atom in the sample, thus obtaining the local environment of each type of atom separately. In the case of an amorphous sample it is convenient to define the environment in terms of the partial radial distribution functions, i.e. the distribution of atoms of a given type relative to an atom also of a given type. We therefore generalize Equation 6 for the EXAFS function on an absorption edge of an atom of type α as:

$$\chi_\alpha(k) = \sum_\beta \int_0^\infty \frac{\mathrm{d}r}{kr^2} P_{\alpha\beta}(r) |f_\beta(\pi)| \times \exp(-2r/\lambda) \sin(2kr + 2\delta_1' + \psi_\beta), \qquad (7)$$

where the sum is over the different types of atom present in the sample, including α. $P_{\alpha\beta}(r)$ is the radial distribution function (RDF) of atoms of type β relative to atoms of type α. It includes the thermal and disorder broadening of the distribution. In the case of a two-component system such as a nickel–copper alloy we would have three such partial RDFs: P_{NiNi}, P_{NiCu} and P_{CuCu}. The type of atom giving rise to a particular frequency component in the EXAFS signal may be identified by the characteristic energy dependence of the backscattering factor $|f_j(\pi)|$ [20].

A good survey of the relative merits and problems of EXAFS and diffraction techniques in structural studies of amorphous systems has been given by Bienenstock [22].

Substitution of simple forms of $P_{\alpha\beta}(r)$ in Equation 7 gives different forms for the EXAFS function $\chi(k)$. A Gaussian peak gives rise to Equation 6 and this is the form most commonly used. Truncated exponentials also give simple analytic forms for $\chi(k)$ and, since they more accurately represent the effects of hard sphere repulsion may be superior in studies of highly-disordered systems. The question of the form of $P_{\alpha\beta}(r)$ has been discussed by Haensel *et al.* [21] who show that determinations of N_j are sensitive to the assumed shape of the distribution function but that the other parameters are not. This is because the values of N_j and σ_j^2 are highly correlated.

In EXAFS studies our main interest lies in the partial RDFs. The forms of Equations 6 and 7 suggest how these may be obtained in practice. The methods fall into two main groups: real-space analysis, where we work on the Fourier transform of the spectrum, and k-space analysis, where we work with the EXAFS function itself.

The simplest method of analysis, and the one which was almost exclusively used in the early (1970–75) EXAFS work, is to Fourier transform $k\chi(k)$ with respect to $\sin(2kR)$ or $\exp(-2ikR)$, where i is $\sqrt{-1}$: the latter is to be preferred since taking the modulus of a complex transform removes some of the problems associated with taking a transform over a finite data range, problems which severely limit the usefulness of many of the early EXAFS analyses. Such a transform gives $\Sigma P_{\alpha\beta}(r)$, with the R values of the peaks slightly shifted due to the effects of the extra phase contribution $2\delta' + \psi$, weighted by the various backscattering factors and including truncation effects from the finite data range. These last may be removed, at the cost of some peak broadening, by use of a suitable window function. Such a simple transform is useful when used for preliminary analysis since it fixes the interatomic distances fairly well and gives a good idea of the amount of information in the spectrum.

To improve the analysis we can weight the experimental spectrum using calculated backscattering factors and take the Fourier transform with respect to $\exp(-2ikR - 2\delta' - \psi)$ using calculated phase-shifts. In complex systems the scattering parameters we choose for this are of course those of the chemical species which gives the dominant contribution to the spectrum. This modification gives good RDFs and has been used extensively by the groups working on the Daresbury synchrotron and others [19, 23–25]. A more common method of proceeding is to use phase-shifts and amplitudes obtained empirically from an EXAFS study of a crystalline material of known structure and containing the same types of atom as the sample of interest. The procedure for doing this is described below. Such phase-shifts and amplitude factors have been shown to be transferable between materials of similar composition, although the method is not without its dangers [26].

The detailed structural parameters of the sample (interatomic distances, co-ordination numbers, etc.) may be obtained by a fit to the Fourier transform of the spectrum. This transform is a convolution of the partial RDFs with a peak function which describes the effects of the other factors in Equation 7. In the analysis technique developed by Hayes [1] this peak function is extracted from the Fourier transform of the EXAFS function of a standard of known structure. The details of the method are given by Hayes [1]. We shall refer to this as the "real space" method of analysis.

The other main method of analysis relies on fitting the experimental EXAFS function χ_α itself in k-space by calculating a spectrum using an assumed set of structural parameters and adjusting these until the best fit is achieved. This is done shell-by-shell (a "shell" of atoms is the set of N_j identical atoms at the same distance R_j from the emitting atom) using the expression given by Equation 6 with calculated phase-shifts and scattering factors and has produced some extremely detailed information. It requires good theoretical scattering data and is rather time-consuming computationally but undoubtedly gives the most detailed structures. It is also the most suitable method for use when the exact expression for the EXAFS function, Equation 5, has to be used [16, 17]. It is also a good method for determining small changes in interatomic distances; say between amorphous and crystalline forms of the same material, or in cases where two shells lie at very similar distances from the emitting atom [23–25, 27]; since even if the calculated scattering parameters are not very accurate, so that the absolute distances determined are inaccurate, the difference

or change in interatomic distance will be exact. The calculated scattering parameters used in this method are usually checked by fitting the EXAFS spectrum of a known crystal standard [23–25].

A modification of this second method of analysis which combines it with the first is also in widespread use. In this, the experimental EXAFS function is first Fourier transformed with respect to $\exp(-2ikR)$. A small part of the resulting real-space spectrum, containing only one peak, is then backtransformed into k-space, the result being the contribution to the EXAFS from atoms lying in a single shell. Such a filtered spectrum from a known standard will give an experimental determination of the energy dependence of the phase factor $2\delta' + \psi$. Knowing this, the period of the filtered spectrum of the unknown sample then gives the interatomic distance and type of scattering atom and a comparison of amplitudes with the standard gives changes in co-ordination number and mean square variation in distance between the reference and test samples. This method was developed by Brown *et al.* [28] and has been extensively used by Rabe *et al.* [29, 30]. The main problem in using it is the need for two Fourier transforms, each taken over a limited data range. Particular care must be taken with the second transform as regards the range of distances included and the window function used and serious difficulties may arise if the sample contains two shells of atoms only a small distance appart. Its major advantage is its computational simplicity, in that no calculated parameters are needed, and its ability to determine bond lengths extremely accurately [30]. We shall refer to this method as the "Fourier-filtering" technique.

All three of the methods described have their merits and their problems and all three have been extensively used in the analysis of EXAFS data taken on a wide range of materials. We shall now consider some of the results obtained for samples of particular interest from a structural point of view.

3. Metallic glasses

Amorphous metallic alloys may be produced in bulk form by cooling from a melt using very high cooling rates, $10^{6\circ}\,\mathrm{C\,sec^{-1}}$ is typical, and special techniques to achieve this on a large scale have now been developed. These amorphous alloys exhibit the usual metallic property of high electrical and thermal conductivity and they may also be ferromagnetic or superconducting. The great technological interest which is presently being shown in these materials is due to the fact that they also possess a high ductility and corrosion resistance and that the ferromagnetic alloys have a very low magnetic coercivity. All of these properties vary to a greater or lesser extent with the composition of the alloy and, since the amorphous state is usually metastable (the true equilibrium state is always the crystalline form, but the transition to this form from the amorphous state is extremely slow at normal temperatures) over a fairly wide composition range, a wide variety of materials with significantly different properties may be manufactured.

Glass-forming metallic alloys can be classified into three basic types [31]:

(a) the simple-metal binaries, such as Cu–Al or $Be_{70}Al_{30}$.

(b) the transition-metal–transition-metal or transition-metal–rare-earth alloys, where a transition metal or rare earth atom with few electrons in its unfilled shell, such as Ti, Zr, Nb, Gd or Tb, is combined with a transition metal with an almost full d-shell, such as Fe, Ni or Cu. These form amorphous alloys over a wide range of compositions about the one-to-one atomic ratio.

(c) alloys containing a transition metal together with metalloid such as Si, Ge, P or B. This is the most important class of the three. These form amorphous alloys over a narrow composition range at or about 20% metalloid content where a deep eutectic exists in the phase diagram.

A full review of the glass-forming metallic systems studied up to 1977 has been given by Donald and Davies [33] and there is also an earlier review by Cargill [34].

All of these materials contain at least two elements, and many of the most interesting contain up to four different atomic types, so the problem of atom identification in the RDF is of crucial importance. To date, most of the characterizations of local structure in metallic glasses have been made using X-ray or neutron diffraction [34] and, as we noted above, these provide only the sum over all the partial RDFs, unless special techniques such as the use of anomalous scattering in X-ray diffraction or isotopic substitutions in neutron diffraction are used. The total RDF obtained as a Fourier transform of the interference function typically shows a well-defined sharp nearest-neighbour peak, containing from 10

to 13 atoms and, further out, a split second-neighbour peak. These RDFs are very like those produced by the dense random packing of hard spheres (DRPHS) model first proposed by Bernal [35]. Most structural models and interpretations have consequently been based on this model. The geometrical constraints imposed by dense random packing explain the overall features of the RDF very well. The first peak is due to spheres in contact, so that it lies at an interatomic distance of 2σ, where σ is the hard sphere radius, whilst the split second peak is due to a combination of contributions from three collinear spheres, giving a peak at 4σ, and from two spheres, one on each side of a layer of spheres in contact, giving a peak at 3.46σ. This simple model may be generalized to include spheres of different radii. The simple hard-sphere model takes no account of chemical ordering effects, but these may be included by relaxing (in a computer simulation) the hard spheres distribution under the influence of atomic pair potentials which have a long range component. Such calculations have been made for simple-metal binary alloys [36, 37] where the pair potentials may be easily calculated.

The major results to be determined from structural studies of metallic glasses are the interatomic distances and whether or not a particular glass shows chemical ordering effects. Interatomic distances may be obtained using any of the experimental techniques mentioned above, but the investigation of chemical ordering requires a knowledge of the partial RDFs. The ability of EXAFS studies to determine these, and to identify the type of scattering atom from the energy dependence of $|f(\pi)|$ is of major significance in determining the atomic arrangement in metallic glasses and in testing proposed models of their structure.

In this section we give a survey of the major results obtained using EXAFS in studies of metallic glasses, comparing these where possible with other data, and endeavour to link them up with physical models of the important atomic interactions to obtain a picture which describes the general structural properties of metallic glasses.

3.1. Simple-metal binary alloys

The simple-metal binary alloys are not of great technical interest and until recently very little work had been done on them. These systems are, however, simplest to deal with theoretically since the interatomic pair potentials may be calculated simply from the well-understood pseudo-potentials [37]. Several such calculations have now been completed [36–38] and experimental studies using diffraction methods are now being undertaken to verify the results of these. The calculations show that very little chemical ordering occurs in these materials and the preliminary experimental results [39] support this view. We may therefore describe these materials in terms of hard-sphere atoms of different radii, interacting weakly via long-range pair potentials. The weakness of the long-range part of the pair potential may be ascribed to the screening of the ion-cores by the nearly-free-electron Fermi sea in which they are imbedded.

3.2. Transition-metal binary alloys

Binary amorphous transition-metal–transition-metal or transition-metal–rare-earth metallic alloys may be produced in bulk in a narrow composition range around the 50%–50% region and as thin film samples (by vapour deposition or sputtering) over a much wider range. They have been extensively studied using EXAFS, for which they are particularly suitable since in most cases the K-edge (for the transition metals) or the L-edge (for the rare earths) are accessible to the X-ray spectrometers in current use [32], so that spectra can be obtained for all the components of the alloy. Detailed information on the local atomic environment can thus be obtained and checked for self-consistency.

3.2.1. Zr–Cu

A good example is the amorphous Zr–Cu alloys studied by Haensel *et al.* [21] and by a group working at Orsay [40, 41]. The zirconium K-edge lies at 18 keV, that of copper at 9 keV, so both are accessible and the wide separation between them allows clear, non-overlapping spectra to be obtained.

Haensel *et al.* [21] analysed the EXAFS spectra of a $Zr_{54}Cu_{46}$ alloy using the Fourier-filtering method [28–30] with a correction applied for the non-Gaussian distribution of interatomic distances [42]. The Fourier-filtered spectra were fitted in k-space using the calculated phase-shifts of Lee and Beni [43] as well as scattering parameters derived experimentally from Fourier-filtered EXAFS spectra from standards. The Fourier transform of the zirconium K-edge spectrum shows two clearly resolved peaks, due to Zr

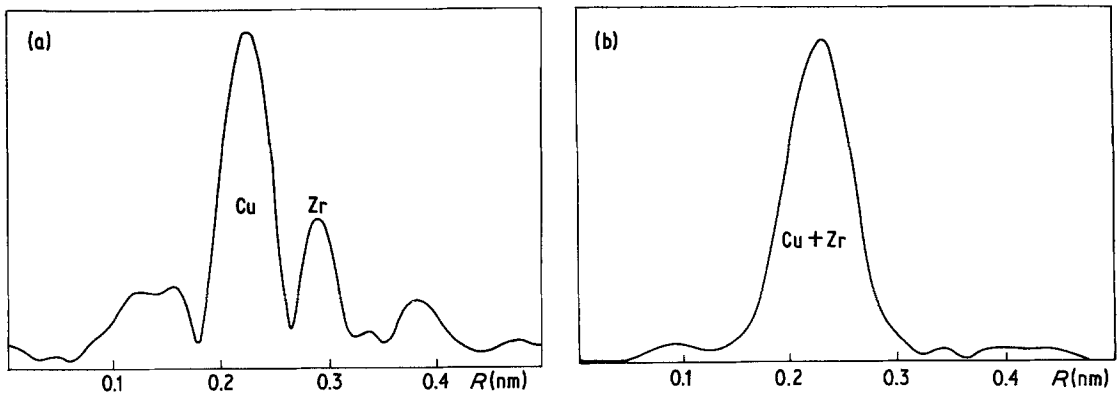

Figure 2 EXAFS-derived partial RDFs for an amorphous $Zr_{54}Cu_{46}$ alloy, after [21]. These were obtained from (a) the Zr and (b) the Cu K-edge spectra and show the local environment of these two types of atom.

and Cu nearest neighbours, whilst that of the copper spectrum shows only one, due to the overlap of the two contributions, (see Fig. 2). Fitting the zirconium spectrum in k-space after Fourier-filtering yields the arrangement of the nearest neighbours: each Zr atom is surrounded by 4.6 ± 0.1 Cu atoms at 0.274 ± 0.002 nm and 5.1 ± 0.1 Zr atoms at 0.314 ± 0.002 nm. These results have been corrected for the effects of the non-Gaussian distribution of neighbouring atoms, a problem carefully considered by Haensel *et al.* who follow the work of Eisenberger and Brown [44].

The EXAFS results agree with X-ray diffraction data [45] except that the interatomic distances are consistently shorter by about 0.001 nm. This is due to the asymmetric pair distribution function: EXAFS measures the position of the peak of the distribution rather than the mean distance [42]. The EXAFS data is also rather more detailed. The neighbours of the copper atom could not be definitely identified owing to the overlap of the two contributions but if the Zr–Cu distance determined from the analysis of the zirconium spectrum were assumed, the copper spectrum gave a Cu–Cu distance of 0.247 ± 0.003 nm.

The numbers of nearest neighbours shows that essentially no chemical ordering is occurring in this alloy. The Zr–Zr distance is the same as in the pure metal (see Table I) whilst the Cu–Cu distance is only slightly shorter. The combination of these results strongly suggests that the bonding in the alloy is metallic and that there are at most only weak chemical effects present.

Somewhat different results have been obtained for the similar alloy $Cu_{60}Zr_{40}$ by Sadoc *et al.* [40]. Using a simple EXAFS theory based on Equation 6, i.e. assuming Gaussian peaks in the RDF, they obtain results which are similar to those of Haensel *et al.* [21] but their best fits do not give spectra which are in good agreement with experiment, particularly at low energy. These problems are probably due to the inadequacy of Equation 6 at low energies, a problem we discussed in Section 2, and so the modification to the structure which they introduce to improve the agreement should be treated with caution. They find that they can get much better agreement with experiment by splitting the nearest neighbour shell into two components, separated by about 0.05 nm, the closer-in component being at the same distance as in the single shell fit and in agreement with the results of Haensel *et al.* The major structural

TABLE I Atomic radii

Atom	Ionic radius (nm)	Atomic radius* (nm)	Covalent radius (nm)
Si	0.271 (– 4)		0.117
Ge	0.272 (– 4)		0.122
B	0.035 (+ 1)		0.080
P	0.212 (– 3)		0.106
Dy	0.091 (+ 3)	0.180	0.159
Tb	0.092 (+ 3)	0.180	0.159
Ti	0.096 (+ 1)	0.145	
Fe	0.074 (+ 2)	0.124	0.117
Ni	0.069 (+ 2)	0.125	0.115
Cu	0.096 (+ 1)	0.128	
Y	0.089 (+ 3)	0.178	
Zr	0.109 (+ 1)	0.158	
Nb	0.100 (+ 1)	0.142	0.134
Pd		0.137	0.128

*Calculated as half the interatomic distance in the metal.

difference between the two fits is to increase the number of Zr neighbours of the Cu atom from two to six and the number of Cu neighbours from four to ten. The degree of ordering present is not changed. The final RDF, a sum of two overlapping Gaussian peaks, closely resembles the asymmetric pair distribution used by Haensel *et al.* The presence of the two subshells may be interpreted as due to packing constraints, it being impossible to get a large number of nearest-neighbours next to the copper atom with the short interatomic distance found in the amorphous alloy. The same explanation may be used for Haensal's wide asymmetric distribution. It is not in general possible to distinguish such fine details of the RDF from the EXAFS results, so either model may be valid.

The results described above suggest that the determination of co-ordination numbers by EXAFS is rather sensitive to the peak shape assumed in the RDF, a conclusion reached both by Haensel [21] and the Laboratory for the Use of Electromagnetic Radiation (LURE) group [40], and this possibility must always be borne in mind, particularly when considering highly-disordered materials. Electron and neutron diffraction studies suffer from similar problems [46]. This is a serious problem since the question of whether or not chemical ordering is occurring in an amorphous alloy depends entirely on the determination of co-ordination numbers. However it appears from both of the papers quoted that the *relative* co-ordinations are less sensitive to this problem, so we may be able to say something useful about the ordering even if the total co-ordination is not well know. The problem may also be solved by a careful study of the low-energy part of the spectrum using Equation 5, since this is much less dependent on the σ_j^2 value than is the high-energy part.

The results of Sadoc *et al.* [40] show that their alloy is chemically ordered to a fair degree, unlike neighbours being preferred. Their analysis of a Ni_2Y alloy in the same paper shows that that alloy is almost totally ordered. Combining these results with those of Haensel *et al.* it appears that the degree of chemical ordering is concentration dependent and we shall consider this point further in the summary at the end of this sub-section.

3.2.2. Cu–Ti alloys

A copper–titanium alloy of approximate composition Cu_2Ti has been investigated by Raoux *et al.* [41] who fit the EXAFS spectrum in k-space using calculated phase-shifts. The phase-shifts were checked by using them in an EXAFS analysis of the crystalline alloy. Both the copper and the titanium K-edges were measured: the copper edge showed strong EXAFS whilst the titanium edge exhibited very little, indicative of a highly-disordered environment for the Ti atom.

The Cu atom was found to have three Cu neighbours at 0.252 nm and six Ti neighbours at 0.274 nm. The nearest neighbours of the Ti atom were all Cu, twelve of them at 0.274 nm with a second shell of about eight Ti atoms at about 0.31 nm. The total co-ordination is about the same in the crystal and the glass. The Cu–Ti distances were considerably more disordered than the Cu–Cu distances, as measured by the fitted values of σ_j^2.

These results show that there is a considerable amount of chemical ordering in this alloy, unlike neighbours being preferred. The interatomic distances are all about 0.005 to 0.010 nm shorter in the glass compared to the crystalline alloy. There is also an observed shift of the Ti K-edge energy between the crystal and the glass.

The amount of ordering present may be quantified by use of an order parameter. The parameter normally used is defined by

$$\alpha = 1 - n^{BA}/(\bar{n}\, c_A) = 1 - n^{AB}/(\bar{n}\, c_B) \quad (8)$$

where n^{BA} is the number of nearest-neighbour A atoms around a B atom, $\bar{n}$ is the average co-ordination number and c_A the concentration of type A. The two forms of α given allow a consistency check to be made on the data. Order parameters for all the alloys described in this sub-section are given in Table II, together with the co-ordinations. Negative values for α indicate a preference for unlike neighbours. α_{max} is the value for complete ordering and is given by $-c_B/c_A$. Neutron and X-ray diffraction data for Cu–Ti alloys [47] show that the chemical ordering is concentration dependent (Table II), being weak for the 50 at %–50 at % alloy and increasing as the copper content, and hence the average electron density increases. All of this information taken together suggests that the driving force for the structure of the amorphous alloy is electron transfer from the copper to the titanium atoms. We shall discuss this further in the summary of this sub-section.

TABLE II Order parameters in transition metal alloys

Alloy	Technique	$\bar{n}$	α	α_{max}	Reference
$Cu_{46}Zr_{54}$	EXAFS	10.4	0	−1.2	21
$Cu_{60}Zr_{40}$	EXAFS	13	−0.25 ± 0.05	−0.7	40
$Ni_{66}Y_{34}$	EXAFS	13	−0.4	−0.5	40
$Cu_{50}Ti_{50}$	Diffn.	11.3	−0.13	−1.0	47
$Cu_{58}Ti_{42}$	Diffn.	11.6	−0.20	−0.7	47
$Cu_{66}Ti_{34}$	Diffn.	12.0	−0.24	−0.5	47
$Cu_{66}Ti_{34}$	EXAFS	12 ± 1	−0.35 ± 0.05	−0.5	41
$Ni_{62}Nb_{38}$	EXAFS	–	−0.5	−0.6	48
$Fe_{66}Dy_{34}$	EXAFS	7 ± 1	−0.5	−0.5	49
$Fe_{66}Tb_{34}$	EXAFS	8 ± 2	−0.5	−0.5	49

3.2.3. Nb–Ni alloys

A study of niobium–nickel alloys by Pettifer *et al.* [48] casts further light on the ordering problem. The EXAFS on the niobium K-edge of the amorphous alloy $Ni_{62}Nb_{38}$ was measured and analysed using an *ab initio* k-space fit. The Nb–Ni distance was determined to be 0.254 nm and the assumption of almost complete chemical ordering was necessary in order to obtain a good fit to experiment. The interatomic distance is considerably less than the sum of the metallic radii (0.267 nm) and is slightly longer than the sum of the covalent radii (0.249 nm). Thus again we see a change from metallic bonding in the crystal to possibly covalent bonding in the amorphous alloy, although electron transfer is a much more likely explanation for the ordering and shortening of the interatomic distance.

3.2.4. $DyFe_2$ and $TbFe_2$

A similar full analysis has been published by Stern *et al.* [49] for the transition-metal–rare-earth compounds $DyFe_2$ and $TbFe_2$ in both amorphous and crystalline forms. Again, the absorption edges of both components can be studied, the iron K-edge being at 7.1 keV whilst the rare earth L-edges lie just above 8 keV. The results for the two alloys are very similar, as might be expected since dysprosium and terbium lie next to one another in the periodic table. In the crystalline state, each rare earth atom is co-ordinated by twelve iron atoms, the distances being Dy–Fe = 0.3036 nm and Tb–Fe = 0.3046 nm. In the glassy state, the Dy atom is surrounded by 7 ± 1 iron atoms at 0.264 ± 0.015 nm and the Tb atom by 8 ± 2 iron atoms at 0.270 ± 0.015 nm. Both alloys show complete chemical ordering. The interatomic distances in the amorphous alloys are very close to the sum of the covalent radii.

The shortening of the interatomic distances on going from the metallic crystal to the glass, together with the complete chemical ordering, has been interpreted [7] as showing that on going from a crystalline to an amorphous state the bonding changes from metallic to a much more covalent type. Charge transfer is an alternative possibility, but the low value of the co-ordination number is more indicative of covalency. Since the tendency towards covalency increases with atomic weight, partially covalent bonding might be expected in an amorphous rare earth alloy where there are no symmetry constraints.

3.2.5. Summary

We have enough structural data on these metallic alloys to give at least a preliminary explanation of the observed structures. It is understandable that those alloys containing rare earth atoms will tend to show a form of covalent bonding, since covalency characteristically increases with atomic weight. We therefore explain the chemical ordering and low co-ordination in these alloys, amorphous $DyFe_2$ and $TbFe_2$, in terms of covalency, although it must be understood that we do not suggest the existence of a full covalent bond as occurs in semiconductors. A better way of expressing our idea might be in terms of the high polarizability of the rare earth atoms. This allows their charge clouds to distort in the amorphous alloy (the requirements of crystal symmetry favour more closely-packed structures, so this does not occur in the crystals) leading to bonding between unlike atoms which is rather like a partially-covalent bond.

The mechanism leading to chemical ordering in the transition metal alloys (both 3d and 4d) is, we suggest, rather different. We can rule out packing considerations as a driving force since it is observed that increasing the copper content in both Zr–Cu

and Ti–Cu alloys increases the tendency to order with unlike neighbours. Since copper is a much smaller atom than either zirconium or titanium (see Table I) packing considerations would favour Cu–Cu neighbours as the copper content increases. The most likely explanation, consistent with all the data, is charge transfer from the atoms with well-filled d-bands (Cu, Ni) to those with an almost empty d-band (Ti, Y, Zr, Nb) leading to a form of partially-ionic bonding. Such bonding would favour unlike neighbours and we would expect the charge transfer to increase as we raise the copper (or nickel) content, since this increases the average electron density, giving a more ordered system. The order parameters listed in Table II show this trend clearly; α increases with the content of the transition metal with the nearly-full d-band. The high co-ordination of the atoms also suggests some kind of ionic bonding. The energy shifts observed for the X-ray absorption edges on going from the crystalline to the amorphous form support this idea, and their size also shows that the charge transfer is small. Thus the ordering effects are not very strong, leading to the partially-ordered structures observed. Extrapolating the trend in Table II suggests that alloys containing less than 50% Cu or Ni would tend to order with like neighbours: confirmation of this awaits further experimental data.

3.3. Metal–metalloid alloys (non-magnetic)

One of the more thoroughly studied types of metallic glass consists of a transition or noble metal host to which approximately 20 at% of a metalloid (B, P, Si or Ge) has been added. At this composition the melting point of the alloy is very low and for a narrow range of concentrations about the eutectic glassy alloys may be formed in bulk by rapid quenching from a melt. Sputtered amorphous films may also be prepared, usually over a wider composition range. The sharpness of the eutectic and the narrowness of the glass-forming region suggest that chemical bonding effects related to the presence of the metalloid atoms, which prefer to form covalent bonds, may be crucial. There is therefore considerable interest in the local atomic environment, particularly that of the metalloid.

Many of the structures proposed for such materials have been based on the model of Polk [50], which is a development of the original DRPHS model of Bernal [35]. Bernal's model contains a fair number of voids between the hard spheres. Polk's idea was to fill these voids with the smaller metalloid atoms, this process making the structure denser and so stabilizing the melt. Moreover, there is one void for every four hard spheres in Bernal's model, which suggests the glass composition which is in fact observed. The model then predicts that each metalloid atom is co-ordinated only to metal atoms, which sit at a wide range of distances from it.

There are some problems with this admittedly very simplified model. In the Bernal model the voids have a wide variety of sizes (compare the similar situation which exists in SiO_2 glasses as investigated using a molecular dynamics simulation [51]) the vast majority of which are small and four-fold co-ordinated. It is only the larger voids, which make up about 10% of the total, which are 8–10-fold co-ordinated and which are large enough to accomodate a metalloid atom. Also, the metalloid atoms are not necessarily smaller than the metal atoms (see Table I). The model takes no account of chemical bonding effects; the complete ordering in the metalloid environment is due to the pre-existing matrix of metal atoms into which the metalloid atoms are constrained to fit, and it is far from clear that the metal atoms should dominate the structure in this way.

An alternative model would have the directional bonding requirements of the metalloid atoms dominating, so that a continuous random network is formed, as occurs in a silicate glass where the modifier ions fit in with the covalent network rather than vice-versa or at higher concentrations are constrained to four-fold co-ordinate the metalloid ions. The sharpness of the dip in the melting point might also be explained in this way. Combining these two models, we get the scheme which is used in computer simulations, where a simple DRPHS system (which may contain several hard-sphere radii) is relaxed under the influence of long-range pair potentials [37, 52].

The two simple models are probably best for physically understanding the main features of the structure of amorphous metal–metalloid alloys, or at least of those alloys where one or the other mechanism dominates, whilst the computer simulation will undoubtedly give the best detailed agreement with experiment for any one particular alloy and also give us quantitative information on the interatomic interactions.

Many diffraction studies have been carried out on metal–metalloid glasses and the results of these are generally consistent with the Polk model, but are not usually sufficiently detailed to absolutely support it. (See, e.g. Sadoc and Dixmier [53].) EXAFS, with its ability to determine partial RDFs and to identify the different atomic species within these should be able to provide much more detailed data on the local atomic environment which will enable us to sort out the dominant effects in these alloys.

3.3.1. Pd–Ge alloys

The EXAFS on the germanium K-edge in Pd–Ge alloys has been measured and analysed by Hayes *et al.* [54]. This group uses the real-space method and in this case the comparison spectra used were those of crystalline Ge and GePd. Two types of sample were investigated: a bulk glass of composition $Pd_{78}Ge_{22}$ and a sputtered amorphous film of $Pd_{80}Ge_{20}$. All data were obtained at liquid nitrogen temperatures. The EXAFS spectra from the two amorphous samples gave identical Fourier transforms out to 0.4 nm, showing that in this material the short range structure is not sensitive to the method of production. (This is not always the case, see, e.g. Greaves *et al.* [55].) The detailed analysis of these Fourier transforms showed that each germanium atom was co-ordinated by 8.6 ± 0.5 palladium atoms at a distance of 0.249 ± 0.001 nm, this shell having a root mean square (r.m.s) half width of less than 0.01 nm. By testing the effects of adding germanium neighbours into a calculated spectrum (a technique which is also used in the analysis of diffraction data [53]) it was determined that the germanium atoms had considerably fewer than one germanium nearest neighbour. This is clear evidence for chemical ordering, since random bonding would lead to two germanium nearest neighbours. This ordering, together with the fact that the Ge–Pd distance is essentially the same as the sum of the covalent radii (see Table I) suggests that covalent bonding is occurring in these materials, the metalloid atoms having a considerable influence on the structure [56], perhaps even giving rise to a continuous random network.

The lack of Ge–Ge neighbours is in agreement with the Polk model also, but the distribution of nearest-neighbour distances is considerably narrower than that predicted by this model. The simple Polk model is indeed unlikely to apply to this material since the covalent radii of germanium and palladium (or even their atomic radii) are essentially equal. Since the two atoms are equal in size the results should be more in agreement with the original Bernal model rather than Polk's development of it. However, such a model is ruled out by the strong chemical ordering effects observed. The only satisfactory way of modelling the structure in terms of hard spheres would therefore appear to be by the use of a computer simulation where the hard sphere structure is relaxed under the influence of interatomic pair potentials which take account of chemical bonding effects.

3.3.2. Ge–Ni alloys

In order to fully investigate the different influences of chemical ordering and atomic size and packing effects, we need to study the changes in local structure which occur when the composition changes. This has been done for amorphous Ge–Ni alloys by Oyanagi *et al.* [56]. These alloys may be made in the form of amorphous sputtered films over a very wide composition range: this particular study used samples containing from 0 to 55 at% nickel. The paper only reports results obtained from the EXAFS on the germanium K-edge, even though the nickel K-edge was also accessible. Interestingly, the whole study was carried out using a conventional X-ray tube rather than a synchrotron source, showing that good EXAFS data may be obtained in the laboratory, with patience! The analysis of the data is complicated by the fact that the Ge–Ge and Ni–Ni distances are very similar (the sums of the covalent radii are 0.244 and 0.237 nm, respectively). A mixture of spectrum fitting in k-space, using scattering data derived from known crystalline materials, and Fourier-filtering was used in the analysis; the co-ordination numbers, atomic types, interatomic distances and mean square variations in distance being taken as variable parameters.

The results are given in Table III. The interatomic distances are generally close to those given by the sum of the covalent radii and do not vary significantly with concentration. We note again that the values determined from an EXAFS analysis are consistently shorter than those obtained from neutron diffraction data [57]. At low nickel concentrations the total co-ordination of the germanium atom remains close to four, indicating that the structure is based on a covalently-

TABLE III Structure of Ge–Ni alloys relative to Ge atom

Ni concentration (at %)	Ge–Ni distance (nm)	No. of Ni neighbours	Ge–Ge distance (nm)	No. of Ge neighbours	Total Ge co-ordination
0.0			0.245 ± 0.002	4.0 ± 0.2	4.0 ± 0.2
10.0*	0.241 ± 0.004	0.5 ± 0.4	0.248 ± 0.003	3.4 ± 0.2	3.9 ± 0.3
23.0	0.231 ± 0.003	1.6 ± 0.2	0.244 ± 0.003	3.2 ± 0.2	4.8 ± 0.4
30.0*	0.238 ± 0.005	1.7 ± 0.2	0.255 ± 0.004	3.2 ± 0.3	4.9 ± 0.5
48.0	0.229 ± 0.003	2.6 ± 0.2	0.241 ± 0.003	3.7 ± 0.2	6.3 ± 0.4
55.0	0.231 ± 0.003	4.0 ± 0.2	0.243 ± 0.003	3.8 ± 0.2	8.1 ± 0.4

*Neutron diffraction results, after Yamada [57].

bonded random network, and at these concentrations the relative numbers of Ge–Ge and Ge–Ni bonds shows that the bonding is random. At high nickel concentrations the total co-ordination of germanium approaches the value of eight or nine given by close-packing models. In this region, Ge–Ge bonds are probably slightly favoured. Studies of the white line, the sharp peak in absorption, which occurs on the germanium K-edge and XPS measurements [58] suggest that at high nickel concentrations there is some p-electron transfer to the metal atoms. This electron transfer will weaken the covalent germanium network and eventually destroy it.

A study of the concentration dependence of the germanium co-ordination shows that the four-fold network disappears rather abruptly at about 20 to 25 at% nickel (Fig. 3). This value correlates well with the electrical behaviour of these alloys: they are semiconducting until the nickel concentration reaches about 25 at%, as are the Fe–Ge alloys [59], above which they are metallic conductors. We may combine all the data and postulate that when the nickel content is below about 25 at% the main feature of the structure is a continuous random network, based on four-fold co-ordinated germanium, which is semiconducting. At about 25 at% nickel content, the charge transfer to the nickel moves the Fermi level into a band of extended states, which makes the material a metallic conductor. This change effects the already weakened covalent bonds and the result is an abrupt change to a close-packed form.

3.4. Ferromagnetic amorphous alloys

A large number of different ferromagnetic amorphous alloys may be produced containing about 80% magnetic atoms (Fe, Co, Ni or combinations thereof) together with about 20% metalloid atoms (B, C, P, Si, Ge or combinations of these). These alloys are of major technological interest because their high ductility makes them very easy to work whilst their low magnetic coercivity makes them very useful as low-loss materials for use in the construction of transformer cores and the like. As quenched from the melt they are extremely strong, with fracture strengths approaching the theoretical limit [60], their behaviour under bending stresses tending towards plastic flow rather than fracture.

The magnetic properties of these amorphous

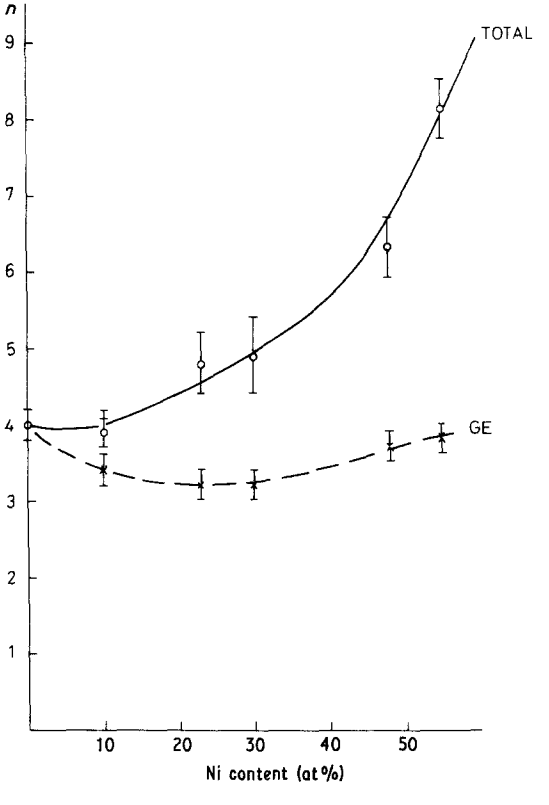

Figure 3 Co-ordination of germanium in nickel–germanium amorphous alloys as a function of nickel concentration.

alloys have been extensively investigated [46]. It is found that the saturation magnetization is only significant for metalloid contents of less than about 20 to 30 at% (which is why we included Ge–Ni in the previous section) and that the Curie temperature drops fairly rapidly as the metalloid content is increased. This is interpreted as being due to the fact that the exchange only operates between metal atoms. The presence of the metalloid both weakens the exchange integral itself [61, 62] and also decreases the number of metal–metal neighbours.

Major EXAFS studies of these alloys have been reported by Wong [7] and by Haensel *et al.* [21]. Analyses have also been completed by de Crescenzi *et al.* [63] and by Cargill [64]. The K-edges accessible to currently used spectrometers are those of the metal atoms and that of germanium, and all have been used. There are considerable differences in the EXAFS analysis techniques used by these authors. Wong [7] used the normal EXAFS formula given by Equation 6 and derived most of his information from the Fourier transform, using crystalline compounds as references to obtain the peak shifts caused by the scattering phase-shifts and changes in the peak heights in the k-space spectrum with temperature were used to derive changes in the mean square variation in distance. These results have been critically reviewed by Cargill [64]. Wong does not obtain co-ordination numbers but he does investigate thermal and annealing effects. Haensel *et al.* [21] use Fourier-filtering to obtain clean data and then fit the spectrum in k-space using calculated scattering data [43, 65]. They find that the assumption of a non-Gaussian distribution of nearest-neighbour distances, caused by the sudden cut-off at small R due to the hard-sphere repulsion, has a major effect on the co-ordination numbers obtained and a small effect on the interactomic distances. Whether this is a real effect, or is an artefact of the fitting procedure (in particular of the Fourier-filtering, since the first peak contains two components), within which the N_j and σ_j^2 are strongly correlated, it is difficult to say at present.

Cargill uses fits in k-space without Fourier-filtering, with calculated scattering data [65] to obtain the structural parameters. In the case of a $Co_{76}P_{24}$ alloy he obtains good agreement using Gaussian peaks in the RDF. One reason for this may be that he fits only the high-energy part of the spectrum, where Equation 6 is much more accurate. Unlike boron, phosphorus has a reasonably high electron scattering factor at high photoelectron energies, so the situation is easier than that considered by Haensel *et al.* [21] and de Crescenzi *et al.* [63] used essentially the same method of analysis as Wong, but do not analyse their data anywhere near as fully.

3.4.1. Fe alloys

From a study of the EXAFS on the iron K-edge, Haensel *et al.* [21] have determined the environment of the iron atom to be 2.2 boron atoms at 0.206 nm and 8.2 iron atoms at 0.255 nm, both components having the rather small r.m.s. half-width of 0.01 nm. All of the values were obtained after correcting for asymmetry effects and are in agreement with X-ray data [66]. The Fe–Fe co-ordination is also consistent with the magnetization data [61, 62]. The Fe–B distance is close to the sum of the covalent radii whilst the Fe–Fe distance is close to that found in metallic iron which is considerably larger than twice the covalent radius of iron. The total co-ordination number of the iron atoms is the line with values predicted by a dense random packing model and the relative numbers of iron and boron neighbours shows that chemical ordering is not significant in the iron environment. That such ordering will be significant for the metalloid environment is suggested by the bond length being given by the covalent radii.

The study of the similar alloy $Fe_{80}B_{10}Ge_{10}$ using the EXAFS on the germanium K-edge, completed by Wong *et al.* [67] produced similar though sparser structural data. The Fe–Ge distance was found to be 0.240 nm, again in agreement with the sum of the covalent radii, and no contribution from Ge–Ge neighbours could be detected.

An X-ray diffraction study of Fe–P alloys by Waseda *et al.* [68] helps to clarify the position, since phosphorus is a strong scatterer and so its contribution to the X-ray RDF is significant. The environment of the iron atom was found to be a close packed structure with no chemical ordering, exactly as given by the EXAFS for Fe–B alloys. The environment of the phosphorus was also close-packed, but with a marked preference for P–P neighbours. The details of the structure are given in Table IVA and B.

3.4.2. Co–P alloys

In a very recent paper, Cargill [64] has analysed

TABLE IVA Ferromagnetic metallic glasses containing boron

Alloy	Technique	Neighbour	R (nm)	N	Notes	Reference
$Fe_{85}B_{15}$	Modelling	Fe–Fe	0.272	11.2	Distances fixed by	52
		Fe–B	0.207	1.1	experiment.	
		B–Fe	0.207	6.96		
		B–B	–	–	Forbidden by model	
	Magnetism	Fe–Fe	–	7.8		61, 62
$Fe_{20}B_{20}$	Modelling	Fe–Fe	0.272	10.8	Distances fixed by	52
		Fe–B	0.207	1.5	experiment	
		B–Fe	0.207	6.4		
		B–B	–	–	Forbidden by model	
	Magnetism	Fe–Fe	–	9.6		61, 62
	EXAFS	Fe–Fe	0.246	4.5	Gaussian peak	21
		Fe–B	0.196	1.2		
		Fe–Fe	0.255	8.2	Asymmetric peak	
		Fe–B	0.206	2.2		
$Fe_{75}B_{25}$	Modelling	Fe–Fe	0.272	11.0	Distances fixed by	52
		Fe–B	0.207	2.0	experiment	
		B–Fe	0.207	6.9		
		B–B	–	–	Forbidden by model	
	Magnetism	Fe–Fe	–	10.9		61, 62

TABLE IVB Ferromagnetic metallic glasses containing phosphorus

Alloy	Technique	Neighbour	R (nm)	N	Notes	Reference
$Fe_{82}P_{18}$	X-ray Diff.	Fe–Fe	0.261	10.7		66
		Fe–P	0.238	2.6		
		P–Fe	0.238	8.1		
		P–P	0.340	3.5		
$Fe_{80}P_{20}$	Modelling	Fe–Fe	–	10.2		52
		Fe–P	–	2.0		
		P–Fe	–	8.4		
$Co_{74}P_{26}$	EXAFS	Co–Co	0.264	10.0	Co K-edge	64
		Co–P	0.228	2.6	Co K-edge	
$Co_{66}P_{34}$	EXAFS	Co–Co	0.248	9.0	Co K-edge	69
		Co–P	0.22	2.0	Co K-edge	
		P–Co	0.22	9.0	P K-edge	
		P–P	–	0.0	P K-edge	

the EXAFS on the cobalt K-edge in a $Co_{76}P_{24}$ alloy. He obtained the structural parameters by fitting the spectrum in k-space using Gaussian peaks as the RDF and calculated scattering data. The detailed results are given in Table IVB. In this alloy the EXAFS is dominated by metal–metalloid correlations (in Fe–B the metal–metal correlations dominate) since phosphorus is a strong scatterer and the Co–P bond lengths are highly ordered. The Co–Co distances are the same as in the pure metal whilst the Co–P distances are close to the sum of the covalent radii. The environment of the cobalt atom shows no ordering, but the small value of the mean square variation in the Co–P distance suggests a fairly strong bonding interaction between the two. Cargill also comments on the difficulty of fitting the EXAFS spectrum of a Fe–B alloy.

A similar alloy, $Co_{66}P_{34}$, has been studied by Lagarde *et al.* [69] who have the advantage of being able to measure the phosphorus K-edge (lying at 2145 eV) using the soft X-ray facility at LURE. Their results for the metal environment are essentially the same as those of Cargill [64]. The analysis of the EXAFS on the phosphorus edge shows that the phosphorus atom is co-ordinated only by cobalt atoms, nine of them lying at 0.22 nm. This is the only EXAFS data for the

metalloid environment in a simple alloy and is at variance with the X-ray diffraction data for $Fe_{82}P_{18}$ obtained by Waseda [68]. The EXAFS is however very clear and the fit exceptionally good, so the completely ordered structure of the phosphorus environment is very likely the correct one. The only explanation for the different structures lies in the different alloy compositions.

3.4.3 Mixed iron–nickel alloys

The information obtained from EXAFS studies of the mixed ferromagnetic alloys is far less precise than that obtained for the simpler alloys because iron and nickel have very similar atomic radii and scattering properties and are therefore hard to distinguish. Mixed alloys containing equal amounts of iron and nickel, together with both boron and phosphorus, have been investigated by Wong [7] and by Haensel *et al.* [21] using the methods of analysis described above. The Fourier transforms of the EXAFS spectra all show a single strong peak at 0.20 nm with a shoulder appearent on the low-R side of this peak in the data from the nickel K-edge only. There is a further weak peak at about 0.35 nm which is very broad: from its position we may say that this is the contribution from the second neighbours, occurring at the position given by dense random packing models, but it is too weak to analyse.

Whilst neither analysis gives results which are as clear as one might wish, it is apparent that the environment of the metal atoms is controlled by packing considerations, exactly as in the simpler alloys. The metal–metalloid distances are close to the sum of the covalent radii again suggesting the presence of some form of chemical ordering. The presence of a shoulder on the Fourier transform of the nickel edge data and its absence from that of the iron edge data suggests that the smaller metalloid atom (boron) is preferentially co-ordinated to the nickel atoms.

3.4.4. Summary

All of these results suggest that the structure around the metal atom in these alloys is that given by a dense random packing model with little or no chemical ordering. The magnetization data [61, 62] for the Fe–B alloys supports this conclusion although they also show that as the metalloid content is reduced below about 15% the packing *decreases*; this is probably a peculiarity of iron-based alloys arising from the fact that pure iron is b c c rather than the close-packed f c c. At very low metalloid content, the amorphous alloys tend to this structure, lowering the total iron co-ordination.

The environment of the metalloid atom is however probably largely controlled by the requirements of covalent bonding: the main evidence for this is the metal–metalloid interatomic distance. The presence of chemical ordering around the metalloid atom is also apparent in several of the studies. The co-ordination of the metalloid atom is higher than a purely covalently-bonded system would allow, at least for high metal content, but the bonding is obviously a major controller of the structure even in those alloys containing only 20% metalloid. In the Ge–Ni alloys with less than about 25% metal content it dominates the structure.

The computer simulations of Boudreaux [52] give results which are in fair agreement with experiment (see Table IVA and B) except as regards the chemical ordering of the metalloid environment. This is due to his model, which specifically excludes metalloid–metalloid neighbours. Whilst this may be good in some cases (such as the Co–P alloy studied by Lagarde *et al.* [69]), it is obviously not a general feature of these alloys. Model calculations must always be scrutinized carefully to ensure that the assumptions of the model do not dominate the outcome too much.

Similarly, we must be careful not to hold too strongly to a simple physical model. We have extensively used the idea of covalent bonding to explain the metalloid environment, and this gives a good explanation of most of the data. However, the magnetic data show that a considerable charge transfer from boron to iron is involved in the Fe–B alloys [61, 62]: this may be interpreted as the rearrangement of charge consequent on the formation of a partial covalent bond but partial ionicity is an alternative model and this may also be used to explain much of the chemical ordering data. The driving forces behind the structures of metal–metalloid glasses are not yet completely determined.

4. Oxide glasses

The classic glass-forming system is based on silica; silicate glasses have of course been known and used for at least two thousand years. Silica is, however, only one example of the very large number of amorphous materials which may be considered

as made up of a topologically-disordered continuous random network of covalently-bonded atoms. Such materials were among the first to be studied using EXAFS with a view to obtaining new structural information. They may be produced either by vapour-deposition or sputtering, which give thin-film samples, or by cooling from the melt to obtain bulk samples. Many of them are semiconductors and are therefore of technical interest, particularly as their electrical properties are strongly composition-dependent. A survey of the electrical properties of these amorphous covalently-bonded materials has been given by Mott and Davis [59].

We shall be concerned here only with the oxide glasses based on silica and the closely related germanate glasses. A full review of the EXAFS results for other covalently-bonded glasses has been given by the author elsewhere [2]. Silica itself (and germania) may easily be prepared as a bulk glass, but for most applications other materials are mixed with it: the addition of an alkali lowers the melting point and the viscosity, making the soda-lime silicates very easy to work; lead increases the refractive index and is added in the production of optical and crystal glass; transition metals colour the glass. Therefore, the practical oxide glass contains many atomic species, and the unique power of EXAFS in the measurement of partial RDFs is particularly useful. A study of the extended structure on the X-ray absorption edges of all the different atomic species in the sample, if it were possible, would give a vast amount of detailed information on the local atomic arrangement which would be extremely useful, especially in understanding the role played by the many network-modifying atoms.

As a preliminary step in understanding the structure of complex glasses it is usual to divide the chemical elements into three classes: the network formers, such as silicon, germanium and arsenic, which form the covalently-bonded network; the network modifiers, such as the alkali metals, which are ionic materials which tend to disrupt the continuous network; and the intermediates, such as the transition metals, which may occur as part of the network or interstitially in the solid. The class into which an atom falls is largely fixed by its ionicity and the structure of network glasses may be understood in terms of the balance between ionic and covalent bonding [70].

Unfortunately most of the network-modifying species, as well as the components of silica itself, are light atoms whose K-absorption edges occur at low energies. At these energies the X-ray absorption coefficient is high and so samples have to be made very thin if the traditional method of measuring the absorption by means of a transmission experiment is used. It is extremely difficult to make such thin samples of a uniform thickness and these practical problems limit transmission experiments to the study of K-edges above about 1500 eV (corresponding to $Z > 14$, silicon: where Z is the atomic number) except under very favourable circumstances (see below). This problem may be avoided by using one of the indirect experimental methods, such as fluorescence or electron-yield EXAFS [71], which were developed for surface studies, or by making measurements in reflection mode [72, 73]. These other methods have only recently been developed and consequently few EXAFS studies of the environment of light atoms have been made. The problems are less severe in the case of germanate glasses, since at least the germanium K-edge is accessible. Information may also be obtained on the environment of transition metal atoms in oxide glasses, since their K-edges are easily accessible. Such partial information is, however, only of limited use.

4.1. Silicate glasses

Silica and sodium silicate glasses are exceptional in that their ductility allows very thin samples to be prepared by blowing films from a molten blob. Such a technique was used by Greaves *et al.* [74] to prepare samples of these glasses approximately 1 μm thick, the optimum thickness for a transmission experiment on the sodium and silicon K-edge. These authors have also successfully made absorption measurements in the energy region above 1300 eV using thin powder samples [75]. Greaves *et al.* [74] describe the EXAFS on the silicon K-edge, which lies at 1830 eV, in amorphous silica, a sodium silicate glass and a sodium calcium silicate glass. The spectra were Fourier-transformed, corrections being made for the phase-shift $2\delta + \psi$, to give a true RDF [19]. The best potential for the calculation of the scattering phase-shifts was determined from a calculation of the EXAFS for α-quartz using several different potentials, that which gave the best fit to the known crystal structure being used in the analysis of the glass spectra.

In amorphous silica, the Si–O bond length was

determined to be 0.159 nm, the same as in α-quartz, and the Si–Si distance was also found to be the same at 0.303 nm. This second-neighbour peak is much weaker in the glass, indicating that although the average Si–O–Si bond angle is the same in the glass and the crystal that there is a considerable amount of random distortion of this angle in the glass. Beyond these two neighbours the structures of amorphous and crystalline silica are completely different. The RDF of amorphous silica derived from the EXAFS spectrum is shown in Fig. 4 and is in reasonable agreement with diffraction data and also with the calculations of Mozzi and Warren [76] which are based on a continuous random network (CRN) model. Detailed curve-fitting of the EXAFS spectra [77] shows that the Si–O–Si bond angle in amorphous silica has an average value of 150°, about the same as in the crystal, with a mean variation about this of ± 15° in close agreement with the model results [76, 78]. Thus the disorder in this material is entirely due to bond-angle distortion, the Si–O bond length being remarkably constant at its crystalline value.

The first two peaks in the RDFs of the two silicate glasses occur at the same distances as in amorphous silica (see Fig. 4): we may therefore deduce that the SiO_4 unit and the Si–O–Si bond angle of about 150° persists in all three glasses. The modifier ions, sodium and calcium, give contributions at around 0.36 nm, in line with the local co-ordination in crystalline silicates and also with the molecular dynamics calculation of Soules [78]. There also occurs in the soda glasses a weak

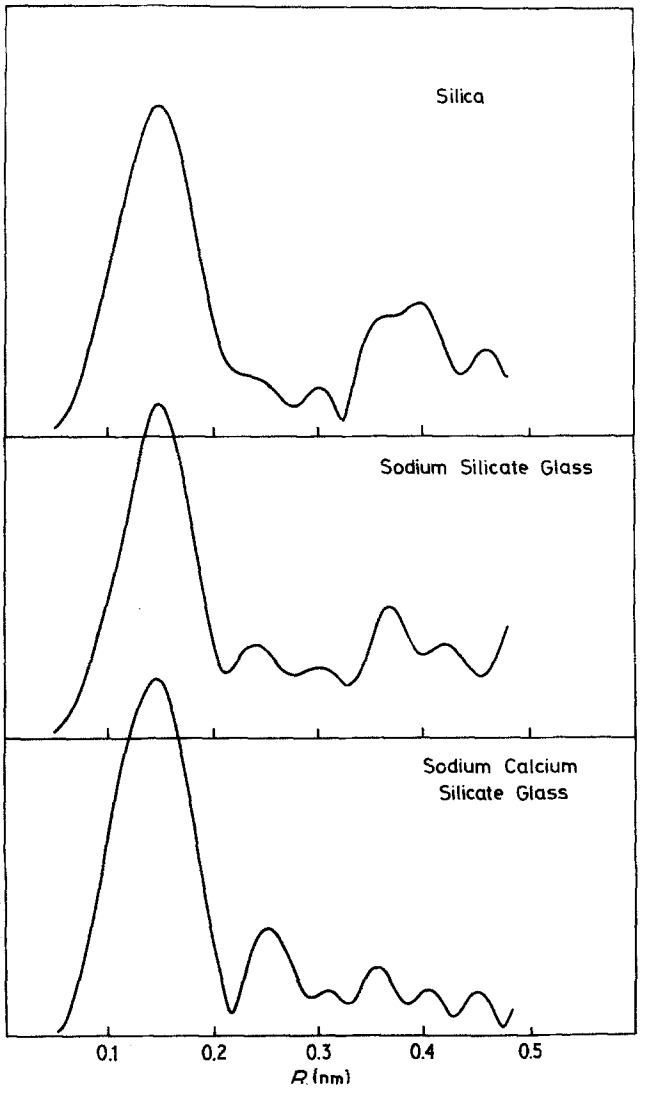

Figure 4 EXAFS-derived partial RDFs relative to silicon in amorphous silica and two silicate glasses, after [74].

peak in the RDF at 0.245 nm which is completely absent in the silica glass. This peak may be a termination ripple in the Fourier transform [19] or it may be a real structure: the analysis has not yet been clarified. If it is real then it probably corresponds to a short Si–Si distance produced by a closing up of the bond angle. Such a feature appears in the molecular dynamics calculation [78]. The bond angle corresponding to the experimental Si–Si distance is 102°, a little less than the calculated value: such a bond angle does not violate packing constraints since the silicon covalent radius is only 0.117 nm [79]. Since this peak does not occur in the pure silica glass in either theory or experiment it must be due to the influence of the modifier ions in distorting the CRN. The calculation shows that these ions cluster round non-bridging oxygen sites, the number of which increases rapidly with modifier content. The breaking of Si–O bonds is therefore presumably the cause of the tighter bond angle.

The EXAFS on the oxygen K-edge at 532 eV in amorphous silica has been measured and analysed by Stohr *et al.* [71] using a secondary electron yield method. Using calculated scattering parameters they determined O–O and O–Si distances: co-ordination numbers could not be obtained from the limited amount of data available. The main interest in this paper lies not in the results, which are rather poor, but in the first successful demonstration of the method, which is very fully discussed.

Greaves *et al.* [77] have also examined the sodium K-edge at 1070 eV in the two silicate glasses and have found well-defined EXAFS. The appearance of EXAFS on the sodium edge demonstrates conclusively for the first time that network-modifier ions in oxide glasses possess a well-defined local environment. Detailed analysis, using curve-fitting in k-space, has shown that this structure is different in the two glasses, reflecting the situation in the crystalline polymorphs. In particular, for sodium disilicate glasses the Na–O distance is 0.23 nm and the co-ordination number is five. (Details are given in Table V.) The same sodium co-ordination is found in crystalline sodium silicates where it corresponds to a trigonal biprism environment. In soda lime silicate glasses the oxygen co-ordination number is six, these atoms being split between two shells at 0.24 and 0.35 nm. Such a split oxygen shell is a common co-ordination for sodium in crystalline ternary silicates [80].

The implications of the above results for the structure of oxide glasses are substantial. It is clear that the sodium ions (and presumably other modifier ions also) play a significant role in fixing the structure of the glass and do not just occupy occasional sites or holes in the SiO_2 network as the conventional Zachariasen model implies [81]. Rather, the structure of silicate glasses should be seen as a natural extension of the layer and chain crystalline structures where the local co-ordinations of network-former and network-modifier atoms are retained but where long-range order is lost, chiefly through random distortion of the bond angles.

Transition metal ions in oxide glasses are generally thought to behave in a manner intermediate between that of the network-formers and network-modifiers [70]. The K-absorption edges of these atoms lie in the medium range of X-ray energies where both spectrometers and synchrotron sources

TABLE V Structure of silicate glasses

Sample	Edge	Neighbour	R (nm) ± 0.002	N ± 1	$\sigma_i^2(10^{-6}\,nm^2)$
α-quartz	Si	Si–O	0.160	4	10 ± 1
		Si–Si	0.306	4	100 ± 10
		Si–O	0.356	4	100 ± 10
SiO_2 glass	Si	Si–O	0.161	4	10 ± 1
		Si–Si	0.317	4	200 ± 70
$Na_2Si_2O_5$ glass	Si	Si–O	0.161	4	10 ± 1
		Si–Si	0.317	4	200 ± 70
	Na	Na–O	0.230	5	56 ± 5
$Na_2CaSi_5O_{12}$ glass	Si	Si–O	0.161	4	10 ± 1
		Si–Si	0.317	4	210 ± 70
	Na	Na–O	0.243	2	140 ± 10
		Na–O	0.286	1	280 ± 50
		Na–O	0.333	3	200 ± 50

are most efficient and so EXAFS studies of the environment of such atoms are straightforward. Two such studies have appeared: that of titanium in silica glass by Sandstrom *et al.* [82] and that on various transition metals and germanium in silica by Petiau *et al.* [83]. Such structural studies are of major interest, particularly in the case of the glasses containing titanium, where the thermal expansion coefficient may be adjusted to near zero by varying the titanium content. The transition metal content of the glass is usually low ($< 10\%$) and so little information on the environment of the metal atom can be obtained using diffraction techniques, which average over all the partial RDFs.

The results of Sandstrom *et al.* [82] on glasses containing up to 10% by weight of TiO_2 show that the generally held view that the titanium occupies a four-fold co-ordinated site (the Ti^{4+} ion being co-ordinated by four non-bridging oxygens) is largely true, but that a proportion of the titanium is six-fold co-ordinated, this proportion increasing with metal content. The four-fold sites have a Ti–O distance of 0.181 nm, the same as in crystalline Ba_2TiO_4, the only crystal with a purely four-fold titanium environment. Such sites account for about 95% of the titanium atoms in a glass containing 7.5% TiO_2, this proportion falling to about 85% when the metal content is raised to 9.5%. The six-fold sites have an octahedral symmetry, the bond length being considerably longer at 0.215 nm. This again is in line with the structure of the various crystals that contain four- and six-fold co-ordinated titanium in a silicate matrix [80]. The interatomic distances are consistent with a model where the four-fold co-ordinated titanium atoms have substituted for silicon atoms whilst the six-fold sites are interstitial. Thus titanium does behave in a manner intermediate between that of a network-former and a network-modifier, tending rather towards the former.

The summary of the results of Petiau *et al.* [83] shows that several other transition metal atoms behave in an intermediate way, the co-ordination of the atom being either four-fold tetrahedral or six-fold octahedral. The co-ordination of the atom is reflected in its ionization state, as determined by the edge shifts of the X-ray absorption. The interatomic distance M–O is generally the same as in the complex crystalline silicates. Zinc is an exception to this general result in that it is only found in four-fold sites [84]. Since it is the only member of the series with a full d-band, this anomalous behaviour is not too surprising [85]. Germanium also only occurs in four-fold sites when added to silicate glasses [83]: it is presumably substituting for silicon in the network.

4.2. Germanate glasses

The most extensively studied (from the EXAFS point of view) glass-former is germania, GeO_2. This is because the K-absorption edge of germanium is easily accessible. Germania was, indeed, one of the first amorphous materials to be studied using EXAFS. This very early paper [86], dating from well before the time when the theory was worked out, shows clearly that the amorphous material resembles the hexagonal crystalline form of GeO_2, where the germanium is four-fold co-ordinated by oxygen rather than the six-fold co-ordinated tetragonal form. A similar situation occurs in silica, SiO_2, where both six-fold and four-fold co-ordinated silicon atoms occur in the crystals but the glass is always four-fold co-ordinated. These results confirm the view that GeO_2 is structurally very similar to SiO_2 and that germanate glasses may serve as an experimentally more convenient analogue of the silicate glasses.

Two EXAFS studies of germania have been published: by Sayers *et al.* [87] who investigated the local structure around the Ge atom; and by Wong and Lytle [88] who were interested in the temperature dependence of that structure. Both obtained a value of 0.174 nm for the Ge–O bond length in the glass, shorter than that in the crystal by 0.01 nm. (N.B. Sayers *et al.* [87] do not take into account the phase-shift $2\delta + \psi$ of Equation 6, so their quoted bond lengths are shorter than the true values by about 0.015 nm in both crystal and glass. We have allowed for this in the results given here.) Wong and Lytle [88] also show that the mean square variation in the Ge–O bond length is considerably *less* in the glass than in the crystal and changes but little with temperature. These two facts taken together show that the GeO_4 unit is considerably more rigid in the glass. This strengthening of the primary covalent bonds is due to the absence in the glass of the back-bonding which occurs in the crystal due to symmetry requirements. This change from a more metallic type of bonding in the crystal to pure covalent bonding in the glass is a characteristic feature of many amorphous solids [2]: we saw a similar process occurring in the metallic glasses.

However, although the first shell is highly ordered in the glass, the more distant shells are considerably disordered, due to the random variation in bond angle that characterizes the CRN, and beyond the second shell the structures of amorphous and crystalline specimens are completely different. Sayers *et al.* [87] suggest that this is a reflection of the more symmetric arrangement (with respect to the neighbouring germanium atoms) of the oxygen atoms in the glass consequent upon the replacement of the partially back-bonded system of the crystal by the purely covalent CRN in the glass. This change in bonding is accompanied by a small increase in the Ge–O–Ge bond angle, from 144° to 148° approximately, and the occurrence of a wide distribution of bond angles. These results are in general agreement with X-ray diffraction results but are of higher resolution.

The structural effects of adding different amounts of lithium, in the form of Li_2O, to a germania glass have been studied by Cox and McMillan [27]. They determined the environment of the germanium atom by fitting the EXAFS on the germanium K-edge in *k*-space using calculated scattering parameters. Only the nearest-neighbour oxygen shell was found to contribute to the EXAFS signal. The detailed analysis showed that this shell was split in the glasses which contained lithium. In pure amorphous germania the germanium was found to be four-fold co-ordinated to oxygen, the bond length being 0.171 nm, in excellent agreement with earlier investigations [87, 88]. In the lithium-containing glasses an extra contribution from six-fold co-ordinated germanium, with a Ge–O bond length of 0.184 nm, was needed to obtain a good fit to the data. The bond lengths of the two sites were independent of lithium concentration. The number of six-fold sites increased steadily with lithium content, tending to saturate at about 25% of the total number of Ge sites (Fig. 5). The results also show that the mean square variation in bond length for both sites are comparable and similar to those found in crystalline materials. All of this is confirmation that the sites are well-defined and accommodated via oxygen bond-bending in the overall network. Here we see a situation where GeO_2 is not analogous to SiO_2. The changes in the structure of the germanate glass as lithium is added (as Li_2O) may be interpreted as a consequence of the extra oxygen atoms entering the network and breaking Ge–O–Ge units. Unlike the situation in silicate glasses, where all the silicon atoms remain four-fold co-ordinated [77], this process is accompanied by a change in the co-ordination of some of the germanium atoms; some of them move into six-fold co-ordinated sites where they are most likely surrounded by non-bridging oxygen atoms, as are the lithium atoms, showing that the network is considerably modified by the presence of the alkali.

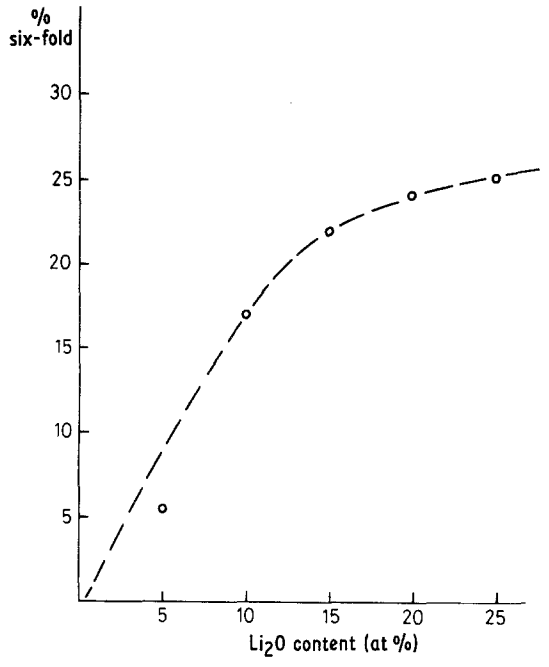

Figure 5 Proportion of six-fold co-ordinated germanium sites in lithium germanate glasses as a function of alkali content.

5. Catalysts

A catalyst is a substance which accelerates a chemical reaction, or alters the relative proportion of different reaction products, without itself being used up in the process. The phenomenon of catalysis is a vital factor in many biological processes and also forms the basis of a large part of the chemical and petroleum industries. It is now also of major importance in the control of pollution, particularly that from motor-car exhaust gases. A review of the structure of some of the major types of catalyst has been given by Sinfelt [89].

Catalytic processes are commonly divided into two classes, homogeneous and heterogeneous. The former term refers to processes in which the cata-

lyst and reactants are present in a single phase, such as a solution. In heterogeneous catalysis the reactants and catalysts are in separate phases, the most common example being that of vapour-phase reactants in contact with a solid catalyst. Catalysts are normally extremely specific, i.e. a given catalyst will only catalyse one, or a few closely related reactions. For catalysis to occur at a surface, as in the case of vapour–solid heterogeneous catalysis, chemisorption of at least one of the reactants is normally required, and it is this stage of the process which, it is generally thought, causes the specificity. For maximum catalytic activity the chemisorption must be fast but not too strong. Nor must it be too weak or else the bonding in the adsorbed reactant molecule will not be sufficiently altered by the adsorption and the reaction rate will not be much different from the non-catalysed rate.

Most catalysts of practical interest are metallic, usually being made up of metals with a high density of states at the Fermi level (transition metals, rare earths and the platinum group) and it is with these that we shall be mainly concerned here. They are characterized by a high specific surface area, the catalyst usually consisting of finely-divided metal particles, either free or dispersed on the surface of a suitable non-reactive carrier such as a refractory oxide. The small size of the catalyst particles causes difficulties for structure determination: X-ray diffraction provides little of use on the small (< 5 nm diameter) particles which are of interest and electron diffraction or microscopy are also of little use, except for particle-size determination. EXAFS, however, due to its atom-specific nature and its dependence on the *local* atomic environment can provide useful structural information.

Given the usual explanation of the origin of catalytic activity, there are three main questions which we may seek to answer by means of EXAFS studies. The first concerns the "bulk" structure of the metal particles, since there are good theoretical reasons for suspecting that this will not be the same in a small particle as in a large crystal [90]. Secondly, we wish to know the nature of the exposed crystal planes or atoms, since this strongly affects the chemisorption process. Finally, since a catalyst is usually in contact with hot gaseous reactants we wish to know of any structural changes which may occur with temperature change.

In this section we shall describe some of the structural information on catalysts that has been obtained using EXAFS analyses. The major part of the section is taken up by a discussion of the results obtained for the platinum group catalysts by Sinfelt and his group and by Joyner; and of the work on copper–ruthenium catalysts due again to Sinfelt. We shall also briefly consider the few other EXAFS analyses of catalyst structure which have appeared in the literature.

5.1. Platinum group catalysts

Finely-divided particles of the platinum group metals, supported on a non-reactive matrix are commonly used as catalysts. EXAFS studies of these materials have been published by Via *et al.* [91] and by Moraweck and co-workers [92, 93], who looked at reduced metal catalysts; and by Joyner [94] and Bassi *et al.* [95] who investigated oxidized samples. The particle sizes are so small, less than 3 nm in diameter, that no other technique is of real use.

The paper by Via *et al.* [91] is a superb example of a careful, rigorous EXAFS analysis. These authors investigated the structure of small particles of osmium, iridium and platinum dispersed on silica or alumina supports, the samples containing about 1 wt% metal. These were carefully reduced in a hydrogen atmosphere. The X-ray absorption data were obtained using the EXAFS 1 line at the Stanford Synchrotron Radiation Laboratory (SSRL), 10^8 photons being accumulated at each energy point to give the very low statistical noise level of 0.01%. The data were then analysed using a Fourier-filtering method, the scattering parameters being obtained empirically from the EXAFS spectra of the pure bulk metals. By comparing data taken at different temperatures on the bulk metals, the authors were able to confirm that they could consistently determine the nearest-neighbour co-ordination to ± 2 atoms and the interatomic distances to ± 0.002 nm. These spectra also showed that the mean square variation in interatomic distance was accurately given by the Debye theory, so long as the correlations in the thermal motion of the atoms were taken into account [19].

The results of the EXAFS analysis are summarized in Table VI. The nearest-neighbour distances of the catalysts on silica supports are in excellent agreement with the values in the bulk metal, which implies that the particles are cubic in symmetry

rather than having the icosahedral structure suggested by theory [90]. All the nearest neighbours are metal atoms. There is also some evidence that interatomic distances of catalysts supported on alumina are reduced, suggesting a stronger interaction with the support in this case. The co-ordination numbers are significantly less than the bulk value of twelve, which is to be expected since these highly dispersed catalysts have a high proportion (about half) of their atoms at the surface of the cluster. The co-ordination numbers are consistent with a particle diameter of order 0.8 to 1.5 nm. The increase in the variation in interatomic distance, σ_1^2, is in line with the behaviour of surface atoms.

The question of the possible contraction in interatomic distance and change of symmetry in very small metal particles, and the shape of these particles, has aroused a great deal of interest. There is no evidence for icosahedral symmetry in the data of Via *et al.* [91] and very little for contraction. The EXAFS analysis of Moraweck *et al.* [92] on platinum particles held in a zeolite matrix does show a contraction of bond length by about 3% (from 0.277 to 0.270 nm). Their particles are rather smaller than those studied by Via *et al.* They also find that the particles are probably a mixture of cubic and icosahedral types.

The most detailed information on the effect of particle size on interatomic distances comes from the EXAFS work of Apai *et al.* [96] who examined copper and nickel clusters in the size range 0.5 to 5 nm supported on graphite. The smallest particles showed a contraction of 10% in interatomic distance which fell to between three and six per cent for particles of 1.5 nm diameter. It therefore appears that contraction is only of significance for the tiniest particles, most catalytic systems being structurally identical to the bulk crystals.

As well as the size of the particles, their shape may also be significant, since it is known that the speed of a catalysed reaction depends on the crystal face exposed by the catalyst [97]. The shape of the particle, and the nature of the exposed face, may be investigated by looking at the contribution of more distant neighbours to the EXAFS spectrum. This problem has been studied by Greegor and Lytle [98] who have shown how the ratio of observed co-ordination number $\bar{N}_j$ to the bulk co-ordination number N_j depends on the shape and size of the particle. The analysis of the contribution to the EXAFS spectrum of shells beyond the first is difficult, since this contribution is weak: Via *et al.* did not attempt such an analysis. However, Greegor and Lytle [98], working with the same EXAFS data, concluded that their catalysts were made up of two-dimensional discs, or rafts, in the case of osmium on silica whilst the iridium catalysts were made up of spherical particles. The analysis gave no clear answer for the platinum catalyst. The nearest-neighbour co-ordinations of Via *et al.* [91] imply that both osmium and platinum samples are rather two-dimensional whilst the irridium catalyst is more likely to be spherical. All of these results are summarized in Table VI.

The results described above were all obtained for reduced catalysts, where the particles are made up exclusively of metal atoms, and where only metal–metal distances contribute to the EXAFS. Oxidized platinum catalysts supported on silica have been studied by Bassi *et al.* [95] and by Joyner [94]. The EXAFS analysis of Bassi *et al.* is rather poor, with severe truncation effects in the Fourier transform which lead to spurious peaks which we feel have in some cases been misinterpreted as neighbour contributions. The results from Joyner show that the only contribution to the EXAFS comes from Pt–O distances: the small particles are therefore completely oxidized. This is interesting in view of the well-known inertness of bulk platinum to oxidation. However, other studies of catalysts [99, 100] support this view and we must therefore conclude that small metallic particles have a different chemical behaviour to large ones. The presence of raft-like structures, where virtually all the atoms are at the surface, would be expected to accentuate this tendency. The data of Bassi *et al.*, where the particle size is much larger, at 5 nm diameter, show an intermediate state, both Pt–O and Pt–Pt distances being observed. These results are again summarized in Table VI.

5.2. Ruthenium–copper catalysts

Ruthenium–copper catalysts, containing equal atomic concentrations of the components, have been studied using EXAFS by Sinfelt *et al.* [101]. Again, this paper is a fine example of a careful EXAFS study. The same methods of analysis were used as in the authors' study of the platinum group catalysts [91] with the additional feature that the chemical type of the nearest neighbour atoms is now of significance. By measuring the

TABLE VIA Platinum group catalysts: reduced catalysts

Metal	Support	Particle size (nm) and shape	R_1 (nm)	R_1 (bulk) (nm)	N_1	σ_1 (10^{-3} nm)	(bulk) (10^{-3} nm)	Reference
Os	SiO_2	0.7 disc	0.2702	0.2705	8.3	5.4	2.7	91, 98
Ir	SiO_2	0.6 sphere	0.2712	0.2714	9.9	6.0	3.0	91, 98
Ir	Al_2O_3	0.6 sphere	0.2704	0.2714	9.9	6.1	3.0	91, 98
Pt	SiO_2	0.6 ?	0.2774	0.2775	8.0	6.1	4.4	91, 98
Pt	Al_2O_3	0.5 ?	0.2758	0.2775	7.2	7.5	4.4	91, 98
Pt	Zeolite	1.2 –	0.2705	0.2775	–	–	–	92
Cu	SiO_2	1.9 sphere	–	0.2275	11.0	–	–	98

TABLE VIB Platinum group catalysts: oxidized catalysts

Metal	Support	Particle size (nm)	Type	R_1 (nm)	N	Reference
Pt	SiO_2	5.0	O	0.203	1.2	95
			Cl	0.238	1.2	
			Pt	0.276	1.4	
Pt	SiO_2	1.7	O	0.194	–	94
			Pt	0.277?	–	

EXAFS on both the ruthenium and the copper K-edges, and using the energy dependence of the backscattering factors (obtained from studies of the pure metals), the type of atom could be accurately fixed.

The results clearly show that the metal particles are segregated, the copper atoms coating the surface of spheres which are almost entirely composed of ruthenium atoms. The main evidence for this is the co-ordination numbers: each ruthenium atom is co-ordinated by 11 ± 1 atoms of which 10 are ruthenium whilst each copper atom is co-ordinated by 9 ± 2 atoms of which five are ruthenium and four copper. These numbers closely fit a model where the small clusters, which are of average diameter 3.2 nm and so have about half of their atoms on the surface, are completely segregated, the copper atoms forming the surface layer and so having a lower average co-ordination than the ruthenium atoms which form the inner parts of the sphere. Chemisorption and X-ray photoelectron spectroscopy studies also suggest that the copper forms a surface skin around the ruthenium atoms. These results are also in agreement with bulk studies which show copper and ruthenium to be immiscible.

5.3. Other EXAFS studies of catalysts

The study of organo-metallic compounds by means of EXAFS is now well-estabilished (see, for example, the Proceedings of the Daresbury Study Weekend, [42]). Only the EXAFS on the absorption edge of the metal can be studied (the absorption edges of light atoms lie at too low energies) but these experiments give information on the environment of that atom, which is a topic of great interest since this data is not available from other techniques as the metal atom is only one in tens or even hundreds of other atoms in the molecule. In the field of catalysts, a cobalt–porphyrin material, which becomes catalytically active for oxygen-reduction upon heat treatment, has been investigated by Joyner [102]. The environment of the cobalt atom was determined by an analysis of the EXAFS on the cobalt K-edge using a k-space fitting procedure. The results show that the porphyrin structure is disrupted upon heat treatment, the active catalyst being a CoN_4 unit. The Co–N distance is unaltered at 0.195 nm. Further, the variation in bond length is the same as in the complete molecule, showing that the fragment is a well-defined entity.

Polymerization catalysts for olefins are frequently based on titanium halides. The structure of these materials is not very well determined since they are extremely unstable, oxidizing readily if in contact with air or damp. A useful EXAFS study of the two titanium chlorides, which form the basis of Ziegler–Natta catalysts, has been made by Vlaic *et al.* [103] using the structure on the titanium edge. Analysis was by Fourier-filtering and fitting in k-space. The interatomic distances were also obtained from the filtered spectra by the method of Martens *et al.*

[104] which gives high accuracy and also serves as a consistency check on the calculated scattering data used. This extra stage of analysis proved to be very useful, as is shown below.

The only contribution to the EXAFS was found to come from the nearest-neighbour shell, and the values of the nearest-neighbour parameters R_1 and σ_1, could be obtained if the co-ordination was assumed from the crystal structure. The Ti–Cl distance in $TiCl_3$ was found to be 0.246 nm, in agreement with the results of X-ray crystallography, but in major disagreement with the earlier EXAFS study of Reed *et al.* [105] who obtained a value of 0.222 nm. This latter value is unreasonable, especially when compared with other known Ti–Cl distances, and is probably due to partial oxidation of the sample in the earlier study, which would lead to a contribution from shorter Ti–O distances. In the case of $TiCl_2$ the bond length was found to be 0.242 nm using a fit in k-space, a value confirmed to ± 0.001 nm using Martens' method. This is different from the crystallographic value of 0.250 nm. However, the quality of the diffraction data is fairly poor, due to experimental difficulties [106], and the EXAFS value is more to be trusted. The shorter Ti–Cl distance corresponds to a shift of the chlorine atom in the crystal away from the totally symmetric position by about 2% of the c-axis: a not improbable variation.

Finally we mention the study of copper-chromium catalysts by Lytle *et al.* [107]. This is only a brief paper but it does show the use of EXAFS in detailing the changes which may occur in a catalyst during use: in this case the catalyst was used for the control of internal-combustion engine exhaust. In a rather different field, the structure of the ion-exchange material zirconium phosphide has been investigated by Alagna *et al.* [108] where a combination of EXAFS and other techniques is used to obtain both the structure and the symmetry of the material in different states.

6. Metallurgy of alloys

The difficulty of determining the local order is one of the barriers to a better understanding of the metallurgy of alloys. The sort of information which we require is the environment of an impurity atom in a host crystal: whether or not impurities, or the dilute component of an alloy, seriously modify the crystal structure of the host in their immediate neighbourhood; whether the components are segregated and if so how; and how this environment depends on the history of the sample. In many cases, we are interested in very dilute alloys and, since the EXAFS spectrum gives information on the local atomic environment of that component whose absorption edge we measure, EXAFS analysis is a very good method for the study of the environment of dilute species. Such studies are virtually impossible using diffraction methods since these sum over all atomic types and the contribution from the dilute species to the signal is swamped by those from the other components.

In this section, we shall describe the results of EXAFS studies of dilute alloys and consider the metallurgical information which may be obtained from such studies. We shall consider data for dilute alloys based on aluminium, the dilute component being copper, zinc or magnesium in concentrations of a few atomic per cent. A more general review of EXAFS studies of dilute species, including thin film and intercalate work as well as dilute alloys and doped semiconductors, has been given by the author elsewhere [2]. The problems we shall consider are the relaxation of the host crystal about an impurity atom and the segregation of the dilute species upon heat treatment, either into clusters or into the extended planar defects known as Guinier–Preston (GP) zones.

Dilute copper–aluminium alloys containing up to 2.5 at% copper have been studied by several groups [109–113] using the EXAFS on the copper K-edge. The spectra were analysed using both an *ab initio* k-space fit with the phase-shifts calculated by Teo *et al.* [65] and also by means of the Fourier-filtering method, where a double Fourier transform of the EXAFS spectrum from a known crystal standard enables empirical scattering parameters to be determined. Empirical and calculated scattering parameters are found to agree closely, except at very low energies, This latter problem is probably largely due to the assumption made by all the authors that the EXAFS function, χ, is given by the simple form of Equation 6. This expression is known to be inaccurate for $k < 50\,nm^{-1}$ since below this value the plane-wave approximation to the photoelectron wavefunction on which Equation 6 is based is no longer valid [23–25]. The Fourier-filtering method with empirical scattering data may be used at lower energies (this is one of its advantages) but we must

look on the empirical scattering data derived from standard crystals as being only an effective parameter and not compare it to theoretical results.

Lengeler and Eisenberger [109] studied alloys containing 0.5 at% copper, which exist in solid solutions, and the two crystalline phases of Al_2Cu. The calculated phase-shifts used were checked against the Fourier-filtered EXAFS spectrum from copper metal. Using the calculated phase-shifts of Teo *et al.* [65] they investigated the structure of crystalline Al_2Cu as a check on the phase-shifts. It was found possible to fit not only the interatomic distances and their mean square variation but also to determine the type and number of the nearest-neighbour atoms with no preliminary assumptions whatsoever. The results obtained were in good agreement with the known crystal structure, the poorest agreement being in the determination of co-ordination numbers: this parameter is strongly correlated with the mean square displacements. This problem is extensively discussed, as are the problems of the finite energy resolution of the experiment and the electron mean free path.

Maeda *et al.* [110] investigated the supersaturated solid solution containing 1.9 at% copper using a Fourier-filtering method, again with Al_2Cu as standard. Their samples were annealed, since they were interested in cluster formation. Fontaine *et al.* [112] used a similar method to study alloys containing 2 to 2.5 at% of copper. These alloys also exist as solid solutions, and here a study of the EXAFS on the copper K-edge gives information on the relaxation of the host crystal around the small impurity atom [113]. On annealing these alloys, about half of the copper content concentrates in the so-called Guinier–Preston zones. These may be considered as extended planar defects, but their structure is not well-known. The analysis of the EXAFS signal shows clearly which of the several simple structural models of these zones is nearest the truth [112]. This first paper by Fontaine *et al.* [112] is a clear and detailed example of a careful EXAFS analysis with all the details of the Fourier-filtering method considered and checked.

6.1. Elastic core effects in solid solutions

The two analyses of the aluminium-copper solid solutions by Lengeler and Eisenberger [109] and Fontaine *et al.* [112] are in essential agreement, although Lengeler and Eisenberger have some evidence for slight clustering of the copper atoms which is not considered by Fontaine *et al.* The results of Maeda *et al.* [110] show a considerable degree of clustering. This is due to their annealing their sample after quenching: the samples used by the other two groups were unannealed. The onset of clustering is interesting in its own right and will be further considered below.

In the unannealed samples the environment of the copper atom was found to comprise twelve aluminium atoms at a distance of 0.275 nm, the mean square variation having the large value of 7×10^{-5} nm^2. The Cu–Al distance is considerably less than the Al–Al distance of the host crystal (0.286 nm) owing to the smaller size of the copper atom. This implies that there must be a considerable amount of relaxation of the crystal around the substitutional copper site and it is this relaxation which is the probable origin of the large variation observed in the Cu–Al distance. No further clear shell contributions to the EXAFS are visible in the Fourier transform, which is uncommon in an essentially crystalline sample [109], indicating that the strain disorder persists over a large distance. By assuming a strain relaxation rate of the usual R^{-2} form, Fontaine *et al.* are able to obtain a fair fit to the higher shell contributions which are weakly observable in the EXAFS signal itself.

The problem of the strain in the crystal has been further considered by the French group [113]. According to Vegard's Law the average lattice parameter of a substitutional solid solution varies linearly with concentration of the dilute component. The variation of this parameter is a macroscopic effect due to point defects (the solute atoms) dispersed at random through an elastic matrix. Using this law, we may calculate the host-solute interatomic distance as a function of concentration via an elastic theory which treats the host crystal as a continuous medium. Such estimates of the amount of distortion are used to analyse small-angle scattering data in order to determine particle sizes or the amount of short-range order.

The results of such a calculation have been compared with the nearest-neighbour distances obtained from an EXAFS analysis for Al–Cu, Al–Zn and Al–Mg alloys by Flank *et al.* [113]. Their results show that although the continuum analysis gets the sign of the change in the first shell distance correct (Cu and Zn atoms are smaller

than, and Mg atoms larger than, the Al atom) it seriously underestimates the magnitude of the change. This is interpreted as being due to the discrete atomic nature of the host crystal and also to the long-range nature of the electronic forces in the case where the solute atom is of different valency to the host atom.

6.2. Cluster birth

The EXAFS results of Maeda *et al.* [110] for Al–Cu alloys shows that annealing induces clustering of the copper atoms before any sign of the presence of Guinier–Preston zones is apparent in the electron microscopy pictures. After annealing a sample containing 1.9 at% copper at 473 K for ten min, the copper atoms were found to have clustered, the EXAFS giving the average environment of a copper atom as three copper atoms at 0.267 nm and nine aluminium atoms at 0.293 nm. The interaction of these two components can clearly be seen in the "beating" effect in the filtered spectrum. There are some weak points in this analysis, marked by the rather large values obtained for the interatomic distances, but the beating in the EXAFS spectrum is clear, so the major conclusions are probably correct.

A similar clustering of zinc atoms in an alloy containing 6.8 at% zinc in an aluminium host has also been observed using EXAFS by Flank *et al.* [113] although in this case the clusters are present even in the as-quenched state. Here, annealing only increases the tendency toward cluster formation.

These clusters have been interpreted [113] as an early stage in the condensation process of small crystallites of a chemical compound, such as Al_2Cu, in the host or of the GP zones. A theoretical analysis of the behaviour of an initially random alloy [114] shows that this segregation occurs in two stages: there is first a rapid condensation of solute atoms into small units, dimers, trimers, etc. up to about ten atoms, followed by a slow growth of these droplets into macroscopic phases. The first stage may be rapid enough to occur during quenching, as in the Al–Zn alloy [113] or may occur only after a little annealing as in the Al–Cu alloys [110]. The second stage requires a long annealing process.

6.3. Guinier–Preston zones

Annealing of aluminium alloys containing about 2 at% copper produces a material in which about half of the copper atoms are concentrated in GP zones [112]. The EXAFS signal on the copper K-edge in the annealed samples is noticeably different from that from the solid solutions, showing that the environment of the copper atoms is different. The signal corresponding to copper atoms in a GP zone was obtained by subtracting the appropriate fraction (~ 0.5) of the solid solution signal from the total signal from the annealed material, and was analysed as before. (Magnetic susceptibility measurements are used to determine the proportion of copper segregated into the GP zones.) The Cu–Al distance was determined as 0.268 nm, the mean square variation in this having the very small value of 2×10^{-5} nm^2. Thus, the structure around a copper atom in a GP zone is considerably more ordered than is the case in a solid solution. Various models of the relative proportions of aluminium and copper in these zones were then tried, these models being those previously put forward in the literature. The EXAFS data clearly ruled out the model where the atomic layer which comprises the planar defect is 100% copper. A good fit to the data was obtained with a structure made up of a layer with a 50–50 composition ratio surrounded by pure aluminium layers. Thus we see that in this case the EXAFS studies, with their ability to concentrate on a particular type of atom, enable us to make much more definite statements about the local atomic environment of dilute species than can be made using the results of diffraction techniques which average over all the types of atom present in a sample, unless special methods are used. A further example of the power of EXAFS methods is provided by the study of tin segregation at grain boundaries in steels carried out by Pardee *et al.* [115].

7. Summary

It is clear from the examples quoted in this review that EXAFS is an extremely powerful tool for the study of the local atomic environment, particularly in amorphous materials. The EXAFS spectrum contains a vast amount of detailed information on interatomic distances, co-ordination numbers, chemical type of neighbouring atoms and mean square variation in bond lengths, and this information may be extracted comparatively easily by means of any one of two or three well-proven analysis techniques, The ability to determine partial RDFs directly from the study of a particular absorption edge and the ease with which the atoms making up these partial RDFs may be

identified make EXAFS studies particularly useful in the study of multi-component systems.

The accurate bond lengths obtained from the analysis of EXAFS spectra for amorphous specimens and the definite identification of atomic types enable us to investigate the bonding in our sample. Thus, in the case of metallic glasses, we were able to demonstrate the existence of chemical ordering in some glasses and its absence in others and so could comment on the different types of bonding in these glasses. In the case of the silicate glasses, the EXAFS spectra from different absorption edges enabled us to investigate the environment of several of the different components of the glass separately. This power of concentrating on one component only was of even greater use in the study of dilute alloys.

The EXAFS technique is, however, limited to the study of close-neighbour structure (out to about 0.4 nm from the emitting atom) by the unavailability for analysis of the low energy parts of the spectrum due to theoretical problems. The simplest methods of analysis using Fourier transform techniques are limited by the range of viability of the simplified expression for the EXAFS function given by Equation 6. When using these techniques the first 100 to 400 eV of the spectrum (the exact amount is dependent on the size of the atoms [23–25]) cannot be simply analysed. If we fit the EXAFS function in k-space using the full expression which takes account of the spherical-wave nature of the photoelectron wavefunction [16] we can go down to within 50 to 100 eV of the absorption edge, but only at the cost of a large amount of computer time. Below this energy multiple scattering effects have to be included.

The Fourier-filtering method of analysis may be used down to very low photoelectron energies since the effects of wave curvature contribute approximately equally in the data from the sample and the crystal comparison material. Thus in this method we obtain an effective value of $2\delta + \psi$ from the standard material which may be used in the analysis but which differs at low energy from the true value due to the effects of wave curvature. This must be borne in mind when comparing empirically determined scattering parameters with calculated values.

This limitation to the higher energy regions of the spectrum limits us to near-neighbour structural analysis since the Debye–Waller factors become increasingly important with increasing interatomic distance, due to the fall off in correlation of atomic thermal motions and the increasing variation in interatomic distances in amorphous materials, and these factors wash out any contributions from distant neighbours. This is less of a problem when using diffraction techniques since the low-q region of the spectrum is analysable in these methods.

Practical limitations on sample thickness and the energy range of X-ray spectrometers also limit the range of atoms which may be studied using EXAFS to those whose absorption edges lie in the medium and hard regions of the X-ray spectrum above about 3 keV: thus we cannot easily study the environment of atoms of atomic number less than about 20 except by the use of indirect methods such as electron-yield EXAFS. There are a few exceptions to this, as we saw in our description of work on silicate glasses, but they are few.

In spite of these limitations, EXAFS has proved extremely useful in the field of materials science, especially in the study of amorphous materials, and particularly when used in conjunction with other techniques such as neutron diffraction and computer simulation. In the near future, EXAFS studies may reasonably be expected to give an astonishing amount of detailed information on the atomic structure of materials.

References

1. T. M. HAYES, *J. Non-Cryst. Solids* **31** (1978) 57.
2. S. J. GURMAN, in "Extended X-ray Absorption Fine Structure" edited by R. W. Joyner (Plenum Press, New York 1981) Chap. 4.
3. R. F. PETTIFER, in Proceedings of the 4th European Physical Society General Conference, 1979" (Institute of Physics, London, 1979) p. 522.
4. F. W. LYTLE, G. H. VIA and J. H. SINFELT, in "Synchroton Radiation Research" edited by S. Doniach and H. Winick (Plenum Press, New York, 1980) p. 401.
5. S. I. CHAN, V. W. HU and R. C. GAMBLE, *J. Mol. Struct.* 45 (1978) 239.
6. O. GUTTERIDGE, in "Extended X-ray Absorption Fine Structure" edited by R. W. Joyner (Plenum Press, New York, 1981) Chap. V.
7. J. WONG, in "Metallic Glasses I" edited by H. J. Guntherodt and H. Beck (Springer-Verlag, Berlin, 1981) p. 71.
8. B. K. TEO and D. C. JOY (EDS) "EXAFS Spectroscopy" (Plenum Press, New York, 1981).
9. R. W. JOYNER (ED) "Extended X-ray Absorption Fine Structure" (Plenum Press, New York, 1981).
10. H. A. BETHE and E. SALPETER, "Quantum Mechanics of One- and Two-Electron Systems" (Springer-Verlag, Berlin, 1959).

11. J. A. VICTOREEN, "International Tables for X-ray Crystallography" Vol 3 (Kynoch Press, Birmingham, 1962).
12. R. DE L. KRONIG, *Z. Physik* **70** (1931) 317.
13. *Idem, ibid.* **75** (1932) 191.
14. *Idem, ibid.* **75** (1932) 468.
15. D. E. SAYERS, F. W. LYTLE and E. A. STERN, *Adv. X-ray Anal.* **13** (1970) 248.
16. C. A. ASHLEY and S. DONIACH, *Phys. Rev.* **B11** (1975) 1279.
17. P. A. LEE and J. B. PENDRY, *Phys. Rev.* **B11** (1975) 2795.
18. S. J. GURMAN, SRC Daresbury Laboratory (UK). Technical Memorandum DL/SCI/TM 21T (1980).
19. S. J. GURMAN and J. B. PENDRY, *Solid State Commun.*, **20** (1976) 287.
20. R. F. PETTIFER and P. W. McMILLAN, *Phil. Mag.* **35** (1977) 871.
21. R. HAENSEL, P. RABE, G. TOLKIEHN and A. WERNER, in "Proceedings of NATO Advanced Study Institute: Liquid and Amorphous Metals" edited by E. Luscher (D. Reidel, Dodrecht, 1980).
22. A. BIENENSTOCK, in "The Structure of Non-Crystalline Materials" edited by P. H. Gaskell (Taylor and Francis, London, 1977).
23. S. J. GURMAN and R. F. PETTIFER, *Phil. Mag.* **B40** (1979) 345.
24. M. A. MAZID, M. T. RAZI, P. J. SADLER, G. N. GREAVES, S. J. GURMAN, M. H. J. KOCH and J. C. PHILLIPS, *J. Chem. Soc. Chem. Commun.* (1980) 1261.
25. G. N. GREAVES, A. FONTAINE, P. LAGARDE and D. RAOUX, S.R.C. Daresbury Laboratory (UK) DL/SCI/R17, (1981).
26. P. H. CITRIN, P. EISENBERGER and B. M. KINCAID, *Phys. Rev. Lett.* **36** (1976) 1346.
27. A. COX and P. W. McMILLAN, *J. Non-Cryst. Solids* **44** (1981) 257.
28. G. S. BROWN, P. EISENBERGER and P. SCHMIDT, *Solid State Commun.* **24** (1977) 201.
29. P. RABE, G. MARTENS, N. SCHWENTER and A. WERNER, *Phys. Rev. Lett.* **39** (1977) 1411.
30. P. RABE, G. TOLKIEHN and A. WERNER, *J. Phys.* **C12** (1979) 1173.
31. H. J. GUNTHERODT and H. BECK (EDS) "Metallic Glasses I" (Springer-Verlag, Berlin, 1981).
32. B. K. AGRAWAL, "X-ray Spectroscopy" (Springer-Verlag, Berlin 1979).
33. I. W. DONALD and H. A. DAVIES, *J. Non-Cryst. Solids* **30** (1978) 77.
34. G. S. CARGILL III, *Solid State Phys.* **30** (1975) 227.
35. J. D. BERNAL, *Proc. Roy. Soc.* **A280** (1964) 299.
36. L. VON HEIMENDAHL, *J. Phys.* **F9** (1979) 161.
37. J. HAFNER, *Phys. Rev.* **B21** (1980) 406.
38. R. KUMARAVADIVEL and R. EVANS, *J. Phys.* **C9** (1976) 3877.
39. H. RUDIN, unpublished work, see [37].
40. A. SADOC, D. RAOUX, P. LAGARDE and A. FONTAINE, *J. Non-Cryst. Solids*, to be published.
41. D. RAOUX, J. F. SADOC, P. LAGARDE, A. SADOC and A. FONTAINE, *J. Phys. Colloq.* **C8** (1980) 207.
42. M. DE CRESCENZI, A. BALZAROTTI, F. COMIN, L. INCOCCIA, S. MOBILIO and N. MOTTA, in "Proceedings of the Daresbury Study Weekend: EXAFS for Inorganic Systems", edited by C. D. Garner and S. S. Hasnain (S.R.C. Daresbury Laboratory, 1981) p. 199.
43. P. A. LEE and G. BENI, *Phys. Rev.* **B15** (1977) 2862.
44. P. EISENBERGER and G. S. BROWN, *Solid State Commun.* **29** (1979) 481.
45. H. S. CHEN and Y. WASEDA, *Phys. Stat. Sol.* **A51** (1979) 593.
46. J. CHANG and D. B. DOVE, *J. Non-Cryst. Solids* **16** (1974) 72.
47. M. SAKATA, N. COWLAM and H. A. DAVIES, *J. Phys. Colloq.* **C8** (1980) 190.
48. R. F. PETTIFER, J. BORDAS, I. DONALD, B. G. LEWIS and H. A. DAVIES, to be published.
49. E. A. STERN, S. RINALDI, E. CALLEN, S. HEALD and B. BUNKER, *J. Magn. Magn. Mater.* 7 (1978) 188.
50. D. E. POLK, *Acta Metall.* **20** (1972) 485.
51. S. K. MITRA and R. W. HOCKNEY, *J. Phys.* **C13** (1980) L739.
52. D. S. BOUDREAUX, *Phys. Rev.* **B18** (1978) 4039.
53. J. F. SADOC and J. DIXMIER, in 'The Structure of Non-Crystalline Materials" edited by P. H. Gaskell (Taylor and Francis, London, 1977).
54. T. M. HAYES, J. W. ALLEN, J. TAUC, B. C. GEISSEN and J. J. HAUSER, *Phys. Rev. Lett.* **40** (1978) 1282.
55. G. N. GREAVES, S. R. ELLIOTT and E. A. DAVIS, *Adv. Phys.* **28** (1979) 49.
56. H. OYANAGI, K. TSUJI, S. HOSOYA, S. MINOMURA and T. FUKAMACHI, *J. Non-Cryst. Solids* **35** (1980) 555.
57. K. YAMADA, unpublished thesis, Tohoku University.
58. K. TAMURA, J. FUKUSHIMA, H. ENDO, S. KISHI, S. IKEDA and S. MINOMURA, *J. Phys. Soc. Japan* **36** (1974) 565.
59. N. F. MOTT and E. A. DAVIS, "Electronic Processes in Non-Crystalline Materials" 2nd edn. (Oxford University Press, Oxford, London, New York, 1979).
60. H. S. CHEN, in "The Structure of Non-Crystalline Materials" edited by P. H. Gaskell (Taylor and Francis, London, 1977).
61. R. HASEGAWA and R. RAY, *J. Appl. Phys.* **49** (1978) 4174.
62. A. P. MALOZEMOFF, M. GRIMSDITCH, J. ABOAF and A. BRAUNSCH, *ibid.* **50** (1979) 5885.
63. M. DE CRESCENZI, A. BALZAROTTI, F. COMIN, L. INCOCCIA, S. MOBILIO and D. BACCI, *J. Phys. Colloq.* **C8** (1980) 238.
64. G. S. CARGILL III, in "Proceedings of the Fourth International Conference on Rapidly Quenched Metals", Sendai, 1981 (Physical Society of Japan).
65. B. K. TEO and P. A. LEE, *J. Amer. Chem. Soc.* **101** (1979) 2815.
66. Y. WASEDA and H. S. CHEN, *Phys. Stat. Sol.* **A49** (1978) 387.
67. J. WONG, H. H. LIEBERMANN and R. P. MESSMER, *J. Mater. Sci.* to be published.
68. Y. WASEDA and H. S. CHEN, *Solid State Commun.*

27 (1978) 809.
69. P. LAGARDE, D. RAOUX and A. FONTAINE, in "Proceedings of the Daresbury Study Weekend: EXAFS for Inorganic Systems" edited by C. D. Garner and S. S. Hasnain (S.R.C. Daresbury Laboratory, 1981) p. 122.
70. R. F. PETTIFER, in "Proceedings of the Daresbury Study Weekend: EXAFS for Inorganic Systems", edited by C. D. Garner and S. S. Hasnain (S.R.C. Daresbury Laboratory, 1981) p. 57.
71. J. STOHR, L. JOHANSSON, I. LINDAU and P. PIANETTA, *Phys. Rev.* **B20** (1979) 664.
72. R. FOX and S. J. GURMAN, *J. Phys.* **C13**, (1980) L249.
73. *Idem, Phys. Chem. Glasses* **22** (1981) 32.
74. G. N. GREAVES, A. FONTAINE, P. LAGARDE, D. RAOUX, S. J. GURMAN and S. PARKE, in "Proceedings of the 1st EPS Condensed Matter Conference, Antwerp 1980" (in press).
75. A. FONTAINE, P. LAGARDE, D. RAOUX and J. M. ESTEVA, *J. Phys.* **F9** (1979) 2143.
76. R. L. MOZZI and B. E. WARREN, *J. Appl. Crystallogr.* **2** (1969) 164.
77. G. N. GREAVES, A. FONTAINE, P. LAGARDE, D. RAOUX and S. J. GURMAN, *Nature* **293** (1981) 611.
78. T. F. SOULES, *J. Chem. Phys.* **71** (1979) 4570.
79. C. A. COULSON, "Valence", 2nd edn. (Oxford University Press, Oxford, London and New York, 1961).
80. W. L. BRAGG and G. F. CLARINGBULL, "Crystal Structures of Minerals" (G. Bell, London, 1965).
81. W. H. ZACHARIASEN, *J. Amer. Chem. Soc.* **54** (1932) 3841.
82. D. R. SANDSTROM, F. W. LYTLE, P. S. P. WEI, R. B. GREEGOR, J. WONG and P. SCHULTZ, *J. Non-Cryst. Solids* **41** (1980) 201.
83. J. PETIAU, G. CALAS, P. BONDOT, C. LAPEYRE, P. LEVITZ and G. LOUPIAS, in "Proceedings of the Daresbury Study Weekend: EXAFS for Inorganic Systems", edited by C. D. Garner and S. S. Hasnain (S.R.C. Daresbury Laboratory, 1981) p. 127.
84. R. F. PETTIFER, in "Proceedings of the 4th E.P.S. General Conference, York, 1979" (Institute of Physics, London, 1979) p. 522.
85. J. WONG and C. A. ANGELL, "Glass: Structure by Spectroscopy" (Marcel Dekker, New York, 1976).
86. W. F. NELSON, I. SIEGEL and R. W. WAGNER, *Phys. Rev.* **127** (1962) 2025.
87. D. E. SAYERS, F. W. LYTLE and E. A. STERN, *J. Non-Cryst. Solids* **8–10** (1972) 401.
88. J. WONG and F. W. LYTLE, *ibid.* **37** (1980) 273.
89. J. H. SINFELT, *Rev. Mod. Phys.* **51** (1979) 569.
90. J. J. BURTON, *Catal. Rev.* **9** (1974) 209.
91. G. H. VIA, J. H. SINFELT and F. W. LYTLE, *J. Chem. Phys.* **71** (1979) 690.
92. B. MORAWECK, G. CLUGNET and A. J. RENOUPREZ, *Surf. Sci.* **81** (1979) L631.
93. B. MORAWECK and A. J. RENOUPREZ, *ibid.* **106** (1981) 35.
94. R. W. JOYNER, *J. Chem. Soc. Faraday I* **76** (1980) 357.
95. I. W. BASSI, F. W. LYTLE and G. PARRAVANO, *J. Catal.* **42** (1976) 139.
96. G. APAI, J. F. HAMILTON, J. STOHR and A. THOMPSON, *Phys. Rev. Lett.* **43** (1979) 165.
97. R. W. JOYNER, B. LANG and G. A. SOMORJAI, *J. Catal.* **27** (1972) 405.
98. R. B. GREEGOR and F. W. LYTLE, *J. Catal.* **63** (1980) 476.
99. T. UCHIJIMA, J. M. HERMANN, Y. INOUE, R. L. BURWELL, Jr, J. B. BUTT and J. B. COHEN, *ibid.* **50** (1977) 464.
100. M. BOUDART, A. ALDAG, J. E. BENSON, N. A. DOUGHARTY and C. G. HARKINS, *ibid.* **6** (1966) 92.
101. J. H. SINFELT, G. H. VIA and F. W. LYTLE, *J. Chem. Phys.* **72** (1980) 4832.
102. R. W. JOYNER, *J. Chem. Soc. Faraday I*, to be published.
103. G. VLAIC, J. C. J. BART, W. CAVIGIOLO, S. MOBILIO and G. NAVARRA, in "Proceedings of the Daresbury Study Weekend: EXAFS for Inorganic Systems", edited by C. D. Garner and S. S. Hasnain (S.R.C. Daresbury Laboratory, 1981) p. 133.
104. G. MARTENS, P. RABE, N. SCHWENTNER and A. WERNER, *Phys. Rev.* **B17** (1978) 1481.
105. J. REED, P. EISENBERGER and J. HASTINGS, *Inorg. Chem.* **17** (1978) 481.
106. E. L. GAL'PERIN and R. A. SANDLER, *Sov. Phys. Cryst.* **7** (1972) 169.
107. F. W. LYTLE, D. E. SAYERS and E. B. MOORE, *Appl. Phys. Lett.* **24** (1974) 45.
108. L. ALAGNA, A. A. G. TOMLINSON, C. FERRAGINA and A. LA GINESTRA, in "Proceedings of the Daresbury Study Weekend: EXAFS for Inorganic Systems" edited by C. D. Garner and S. S. Hasnain (S.R.C. Daresbury Laboratory, 1981) p. 98.
109. B. LENGELER and P. EISENBERGER, *Phys. Rev.* **B21** (1980) 4507.
110. H. MAEDA, T. TANIMOTO, H. TERAUCHI and M. HIDA, *Phys. Stat. Sol.* **A58** (1980) 629.
111. S. K. PRASAD, S. P. SINGHAL, H. HERMAN, J. A. DEL CUETO and N. J. SHEVCHIK, *Scr. Metall.* **13** (1979) 549.
112. A. FONTAINE, P. LAGARDE, A. NAUDON, D. RAOUX and D. SPANJAARD, *Phys. Mag.* **B40** (1979) 17.
113. A. M. FLANK, A. FONTAINE, P. LAGARDE, M. LEMMONIER, J. MIMAULT, D. RAOUX and A. SADOC, in "Proceedings of the Daresbury Study Weekend: EXAFS for Inorganic Systems" edited by C. D. Garner and S. S. Hasnain (S.R.C. Daresbury Laboratory, 1981) p. 70.
114. A. SUR, J. L. LEBOWITZ, J. MARRO and M. K. KALOS, *Phys. Rev.* **B15** (1977) 3014.
115. W. J. PARDEE, W. M. ROBERTSON and M. R. JAMES, *Scr. Metall.* **14** (1980) 1333.

Received 1 January
and accepted 25 January 1982